

Discovery of Highly Selective Inhibitors of Calmodulin-Dependent Kinases That Restore Insulin Sensitivity in the Diet-Induced Obesity *in Vivo* Mouse Model

Christophe Fromont, Alessio Atzori, Divneet Kaur, Lubna Hashmi, Graziella Greco, Alejandro Cabanillas, Huy Van Nguyen, D. Heulyn Jones, Miguel Garzón, Ana Varela, Brett Stevenson, Greg P. Iacobini, Marc Lenoir, Sundaresan Rajesh, Clare Box, Jitendra Kumar, Paige Grant, Vera Novitskaya, Juliet Morgan, Fiona J. Sorrell, Clara Redondo, Andreas Kramer, C. John Harris, Brendan Leighton, Steven P. Vickers, Sharon C. Cheetham, Colin Kenyon, Anna M. Grabowska, Michael Overduin, Fedor Berditchevski, Chris J. Weston, Stefan Knapp, Peter M. Fischer, and Sam Butterworth*

Cite This: *J. Med. Chem.* 2020, 63, 6784–6801

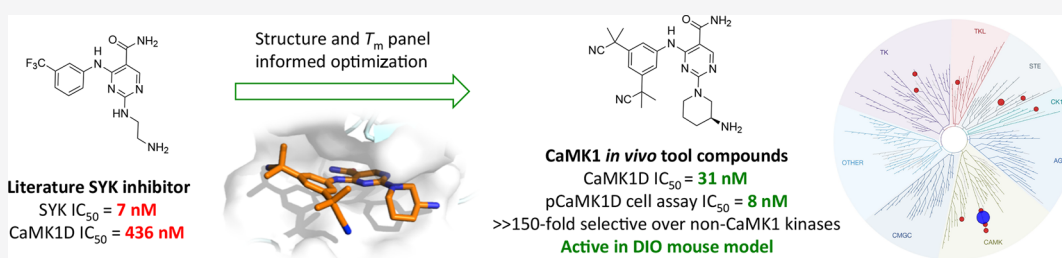
Read Online

ACCESS |

Metrics & More

Article Recommendations

Supporting Information



ABSTRACT: Polymorphisms in the region of the calmodulin-dependent kinase isoform D (CaMK1D) gene are associated with increased incidence of diabetes, with the most common polymorphism resulting in increased recognition by transcription factors and increased protein expression. While reducing CaMK1D expression has a potentially beneficial effect on glucose processing in human hepatocytes, there are no known selective inhibitors of CaMK1 kinases that can be used to validate or translate these findings. Here we describe the development of a series of potent, selective, and drug-like CaMK1 inhibitors that are able to provide significant free target cover in mouse models and are therefore useful as *in vivo* tool compounds. Our results show that a lead compound from this series improves insulin sensitivity and glucose control in the diet-induced obesity mouse model after both acute and chronic administration, providing the first *in vivo* validation of CaMK1D as a target for diabetes therapeutics.

INTRODUCTION

The CaMK1 family of calmodulin-dependent kinases are widely expressed including in hepatocytes, endothelia, immune cells, and the CNS.^{1,2} There are four CaMK1 isoforms with high similarity in the kinase domain, especially the ATP binding site, but that differ in their overall structure and tissue distribution.

Single-nucleotide polymorphisms in the CaMK1D locus are associated with increased incidence of diabetes in a large number of genome-wide association studies (GWAS).^{3–6} While these variations are noncoding, it has been demonstrated that the diabetes-associated polymorphism rs11257655 increases FOXA1 transcription factor binding and thereby increases CaMK1D protein expression in multiple cell models.⁷ A direct role for CaMK1D in glucose processing has been observed following knock-down of commonly observed GWAS-identified proteins in primary human hepatocytes.⁸ In this model, treatment with CaMK1D siRNA results in loss of nuclear

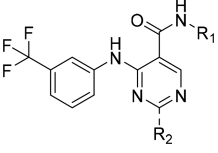
translocation of the established diabetes target CRTCL2/TORC2^{9–11} and is associated with decreased gluconeogenesis and increased glycogen deposition.

Increased CaMK1D expression is also implicated in triple-negative breast cancer (TNBC). Large-scale genomic/transcriptomic analyses of breast tumors indicate that gains at the 10p13 locus, which spans the CaMK1D gene, are observed in 80% of TNBC tumors¹² with high occurrence in estrogen receptor-negative and TNBC tumors of younger patients.¹³ In a separate study, biopsies from 172 breast cancer patients showed

Received: January 21, 2020

Published: May 20, 2020



Table 1. Structure–Activity Relationships of Pyrimidine Amides^b


| Compound | R ₁ | R ₂ | <i>T_m</i> shift (°C) | | | | | | IC ₅₀ (μM) | |
|----------|----------------|----------------|---------------------------------|----------------|----------------|-----------------|-----------------|-----------------|--|--------------------|
| | | | CaMK1D | SYK | DAPK3 | GSK3β | CaMK4 | DCLK1 | CaMK1D | SYK |
| 1 | H | | 5.44 (0.58) | 7.51 (0.09) | 4.05 (0.29) | 3.4 (0.44) | 1.34 (0.28) | 0.11 (0.25) | 0.456 ^a 0.432 (0.084) | 0.007 ^a |
| 2 | Me | | 0.12 (0.3) | - | 1.36 (0.16) | -0.27 (0.39) | -0.18 (0.18) | -0.53 (0.15) | - | - |
| 3 | H | | 7.35 (0.4) | 5.13 (0.17) | 4.48 (0.13) | 0.84 (0.13) | 2.13 (0.21) | 0.10 (0.07) | 0.851 (0.160) | - |
| 4 | H | | 2.43 (0.08) | - | 2.70 (0.27) | 0.70 (0.16) | 3.36 (0.08) | 0.11 (0.14) | 3.49 ^a | - |
| 5 | H | | 4.68 (0.11) | - | 3.45 (0.31) | 0.76 (0.19) | 2.21 (0.1) | 0.08 (0.23) | - | - |
| 6 | H | | 9.84 (0.17) | 8.59 (0.34) | 6.69 (0.11) | 2.31 (0.13) | 4.94 (0.08) | 1.08 (0.04) | 0.485 (0.017) | - |
| 7 | H | | 6.84 (0.07) | 6.82 (0.39) | 4.63 (0.03) | 1.70 (0.12) | 3.36 (0.14) | 0.95 (0.05) | 1.35 (0.018) | - |
| 8 | H | | 10.5 (0.04) | 9.05 (0.36) | 7.01 (0.01) | 2.50 (0.16) | 5.09 (0.15) | 1.1 (0.08) | 0.179 ^a 0.186 (0.027) | 0.087 ^a |

^aCompounds tested at Reaction Biology, $n = 1$. ^bAll data represent mean of at least $n = 3$ independent experiments with standard deviation in parentheses, unless otherwise noted.

significant gains at the 10p13 locus among basal-like tumors, leading to CaMK1D overexpression at transcriptional and protein levels.¹⁴ When expressed in nontumorigenic mammary epithelial cells (MCF10A), CaMK1D was found to lead to transformation, increasing proliferation and inducing a mesenchymal-like phenotype.¹⁴ Mouse models also corroborate the effect of overexpressing CaMK1D on altered cell proliferation and apoptosis.¹⁵

Despite the emergence of CaMK1D as a potentially important therapeutic target, there are no known selective CaMK1 inhibitors. We therefore sought to develop potent and selective inhibitors of this class of kinases for use in target validation experiments, ahead of further translational studies.

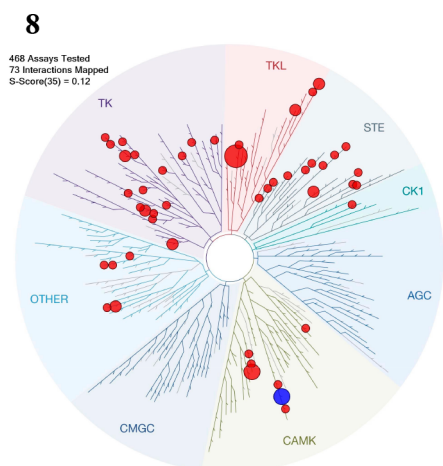
RESULTS AND DISCUSSION

Compound 1 and derivatives thereof have received significant attention as inhibitors of spleen tyrosine kinase (SYK) and may have utility in the treatment of autoimmune disease or lymphomas.^{16–19} Previously published selectivity data shows compound 1 to have inhibitory activity against CaMK1D,²⁰ and as such we selected this as the basis for a structure-based drug discovery campaign, with the aim of improving the potency and selectivity of compounds from this series toward CaMK1D. We

initially examined the compound-induced shift in the thermal denaturation midpoint (T_m) of a small panel of kinases, in order to allow rapid quantification of the binding to both CaMK1D and off-target kinases (Table 1). Initial chemical efforts focused on alterations in the primary amide and amine regions, resulting in compounds 2–6, which demonstrate comparatively steep structure–activity relationships when either the primary amide or primary amine are substituted. Substitution of the secondary amine to give compound 3 is well tolerated and results in an apparent improvement in kinase selectivity, with further derivatization leading to compound 6, which demonstrated a higher T_m shift against CaMK1D and improved selectivity relative to earlier compounds. Separation of the enantiomers of this compound led to compounds 7 and 8, the latter of which has previously been reported as a SYK inhibitor¹⁷ but has higher activity against CaMK1D than its enantiomer and demonstrates a more favorable activity profile relative to compounds 1 and 2 in both T_m and enzymatic assays.

Based on these results, we evaluated the pan-kinome selectivity of 8 in a competitive binding assay at 1 μM, which demonstrated a somewhat targeted profile. CaMK1D and SYK are among the 11 wild-type kinases inhibited by >90% in this

format, supported by subsequent enzymatic selectivity data against selected targets (Figure 1 and SI).



| Kinase | % residual probe binding at 1 μM^a | Enzyme IC_{50} (μM) ^b |
|---------|---|--|
| RIPK4 | 0.9 | 0.092 |
| CaMK1D | 2.0 | 0.179 |
| PIM1 | 2.7 | 0.053 |
| TAK1 | 5.7 | 0.356 |
| CK2a | 6.5 | 9.131 |
| MEK5 | 7.3 | 0.240 |
| PIP5K1C | 8.1 | - |
| CSF1R | 8.6 | 0.168 |
| MLK3 | 8.9 | 0.052 |
| BLK | 9.5 | 0.057 |
| SYK | 9.6 | 0.087 |

Figure 1. Selectivity data against selected wild-type kinases for compound 8. ^aCompounds tested at Eurofins DiscoverX, $n = 1$. ^bCompounds tested at Reaction Biology, $n = 1$.

As expected the CaMK1D-bound crystal structure of compound 8 (Figure 2) shows that the compound binds at the ATP binding site in a type-1 fashion. A comparison of the binding mode of related compounds in SYK (e.g., PDB: 4RX9)

demonstrated a slight shift in binding mode resulting from differences in the conformation of the loop at residues 163–165 (corresponding to 510–512 in SYK) as well as a flip in the orientation of the aniline *meta*-substituent in CaMK1D to occupy a pocket adjacent to L100 at the edge of the hinge region. The L100 pocket appears significantly larger in CaMK1D than the majority of the observed off-targets where structural data was available. In addition, the second *meta* region that is not utilized by 8 is close to the potentially flexible side chain of E105. We hypothesized that flipping of the orientation of the aniline allows the ligand to avoid the L100 pocket when binding to some off-target kinases. This led to the design of compound 9 that removes this ambiguous binding mode by occupying both the L100 and E105 regions.

This bis-*meta* substitution pattern was well tolerated by CaMK1D when assessed by T_m shift and resulted in a significant decrease in the binding to off-targets including SYK (Table 2). Further SAR studies identified that a wide range of functional groups can be tolerated at the L100 pocket, with introduction of groups with a wide range of lipophilicity and bonding potential able to maintain or even enhance binding and selectivity (Table 2).

The binding affinity and selectivity for CaMK1D were further improved by combining these structural features in symmetrical and unsymmetrical bis-*meta* substituted anilines, especially those containing substituents that place electron density above and below the aniline ring plane. The clearest example of this is compound 14, which is too lipophilic to be a useful lead compound but nonetheless exhibits a very high T_m shift with CaMK1D and negligible off target binding. Evaluation of 14 in pan-kinome selectivity assay reveals highly specific binding to CaMK1D and the closely related CaMK1A and CaMK1B, again supported by enzymatic evaluation (Figure 3 and SI).

Our hypothesis is that the disconnect between the apparent high binding of 14 observed by T_m shift and the competitive binding assay at DiscoverRx, compared to the lower activity in competitive inhibition assays, relate to its poor physicochemical properties, which may lead to compound losses during serial dilution.

Despite the issues with properties in this specific example, we believed 14 demonstrated the potential to achieve high selectivity in this series and therefore sought to combine this selectivity with improved potency and physical properties by exploiting the wide SAR scope at the aniline *meta* positions. Subsequent evaluation of a wide range of aniline substituents

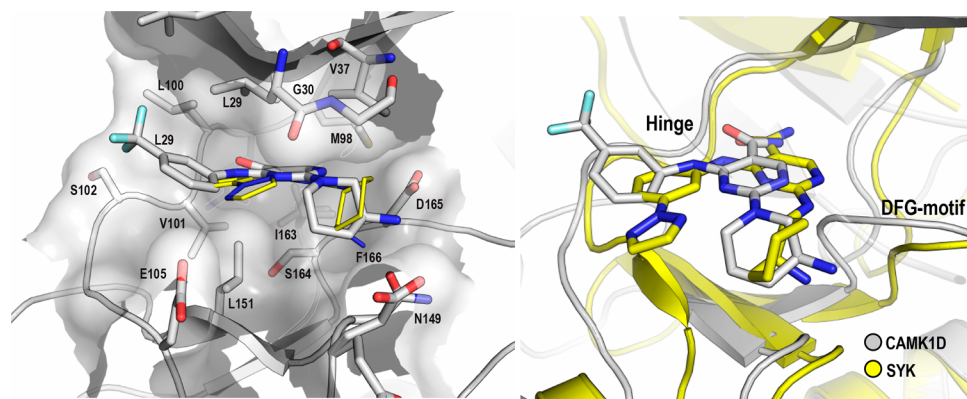
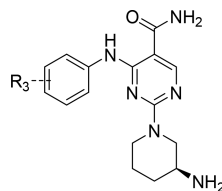


Figure 2. Compound 8 bound to CaMK1D (6T6F, white) and overlay with related SYK structure (4RX9, yellow). Important residues and inhibitors are shown in stick representation. For better visibility, the P-Loop has been made transparent.

Table 2. Effects of Varying Aniline Substitution on Potency and Selectivity^a

| compd | R ₃ | T _m shift (°C) | | | | | | CaMK1D enzyme IC ₅₀ (μM) |
|-------|-------------------------|---------------------------|--------------------------|-------------|-------------|-------------|-------------|-------------------------------------|
| | | CaMK1D | SYK | DAPK1 | CK2a | ABL | PIM1 | |
| 8 | 3-CF ₃ | 10.5 (0.04) | 9.05 (0.36) | 5.92 (0.45) | 3.77 (0.12) | 5.02 (0.36) | 8.32 (0.28) | 0.186 (0.027) |
| 9 | 3,5-diCF ₃ | 13.3 (0.09) | 4.13 (0.57) | 6.07 (0.06) | 5.89 (0.1) | 3.88 (0.24) | 3.98 (0.05) | 0.455 (0.451) |
| 10 | 3- <i>t</i> Bu | 9.61 (0.16) | 4.58 ^b (0.33) | 3.02 (0.09) | 3.02 (0.56) | 2.27 (0.22) | 2.09 (0.44) | 0.277 ^c (0.053) |
| 11 | 3-SO ₂ Me | 7.85 (0.09) | 5.23 (0.18) | 4.21 (0.09) | 5.11 (0.02) | 5.33 (0.09) | 1.78 (0.65) | 0.101 (0.07) |
| 12 | 3-Ph | 11.9 (0.26) | 9.32 (0.29) | 4.81 (0.11) | 3.79 (0.01) | 4.5 (0.26) | 4.96 (0.06) | 0.047 (0.026) |
| 13 | 3-(2-cyano <i>i</i> Pr) | 7.76 (0.24) | 5.00 (0.28) | 3.32 (0.39) | 9.51 (0.19) | 2.85 (0.28) | 1.3 (0.2) | 0.096 (0.05) |

^aAll data represent mean of at least $n = 3$ independent experiments with standard deviation in parentheses. ^bMeasured on racemic compound. ^c $n = 2$.

generally validated our hypothesis that “bulky” substituents are favored for both potency and selectivity.

This work led to compounds **15–18**, which show good binding and selectivity in both T_m and enzymatic assays. Selected compounds were assessed for their ability to inhibit autophosphorylation of CaMK1D at activation loop residues serine 179 and threonine 180 in overexpressing MDA-MB-231 cells. This data demonstrated that the inhibitors have limited cell drop-off for compounds with no additional H-bond donors or basic centers (Table 3). Pan-kinome screening data on **18** (Figure 4) shows that the high selectivity of **14** can be maintained in compounds with more favorable physicochemical properties, with enzymatic data on identified off-targets demonstrating >150-fold greater activity against CaMK1D than all non-CaMK1 kinases.

The *in vitro* pharmacokinetic profile of **18** reveals generally favorable properties with high solubility, low metabolism, and moderately high plasma protein binding (PPB), but low permeability with some evidence of efflux in the CaCo2 model (Table 5). This low permeability does not appear to impact either cellular activity or oral pharmacokinetics, where **18** shows good bioavailability in mice and rats despite moderately high clearance.

The oral pharmacokinetic profile of **18** in mice scaled well at doses up to 100 mg/kg, and the PPB-adjusted cover over cellular IC₅₀ observed suggested that this compound may be suitable for *in vivo* target validation studies (Figure 5).

In order to improve the potential utility of these compounds, we sought to identify a lead compound with improved potency and reduced clearance in order to allow for greater cover in the *in vivo* experiments at reduced doses. In common with **18**, a large number of compounds from this series demonstrated high solubility, low A–B/high B–A CaCo2 permeability and moderate to low metabolism in mouse microsome and hepatocyte assays. However, the *in vivo* clearance of the compounds was often greater than estimated liver blood flow, suggesting that hepatic metabolism is not the key driver of clearance in mouse.

A more detailed evaluation of the *in vivo* pharmacokinetics of **18** revealed a similar picture. Despite its high *in vivo* clearance, metabolite identification studies on rat *ex vivo* plasma samples reveal only low levels of metabolites, resulting from oxidation, acetylation, or amide hydrolysis (potentially subsequent to

acetylation), while analysis of urine collected from **18** dosed rats reveals that renal excretion of unchanged drug at least partially contributes to clearance.

Despite the poor predictivity of the *in vitro* pharmacokinetic assays, optimization of the aniline region of the compounds was continued, relying on *in vivo* studies to distinguish compounds that showed suitable *in vitro* activity profiles. This work led to the finding that compounds containing 4-pyridyl substituents such as that seen in **19** exhibited retained or enhanced activity in CaMK1D enzyme and cell assays with similar selectivity (Figure 6, Table 4) but reduced *in vivo* clearance. Examination of the structure activity relationships around this structural change revealed similar SAR to that observed with the anilines. Our hypothesis is that the pyridyl nitrogen is protonated in the bound state, supported by experimental data revealing that **19** is dibasic, with pK_a values of 8.7 and 7.5 for the primary amine and pyridine, respectively.

The increased potency and higher *in vivo* blood concentrations seen with **19** result in significantly improved free cover over the cellular IC₅₀ in mouse (Figure 7), and consistent with the low CaCo2 A–B/high B–A seen with this compound, the free plasma to brain ratio is ≤ 0.01 at all time points to 24 h. The compound retains high pan-kinome selectivity; however the move to secondary (i.e., isopropyl) substituents does result in a reduction in selectivity over MEK5 in both affinity and biochemical assays. These findings are reflected in the CaMK1D bound crystal structures of compounds **18** and **19** (Figure 8), which show the isopropyl groups in **19** occupying a low-energy conformation with the methyl groups out of the plane of the aryl ring, potentially avoiding unfavorable interactions with the protonated pyridine.

As expected from the high active site homology in the CaMK1 family, both **18** and **19** show limited selectivity between CaMK1A, CaMK1B, CaMK1D, and CaMK1G. More detailed secondary pharmacology screening with **18** and **19** reveals some evidence of hERG and CYP450 inhibition (Table 5) with the compounds demonstrating ~300-fold selectivity over hERG based on cellular IC₅₀.

Initial evaluation of the *in vivo* efficacy of these inhibitors was conducted in mice with diet-induced obesity (DIO mice), which demonstrate impaired glucose control mediated by reduced sensitivity to insulin. Compound **18** was selected for these studies due to its high kinome selectivity, with sampling

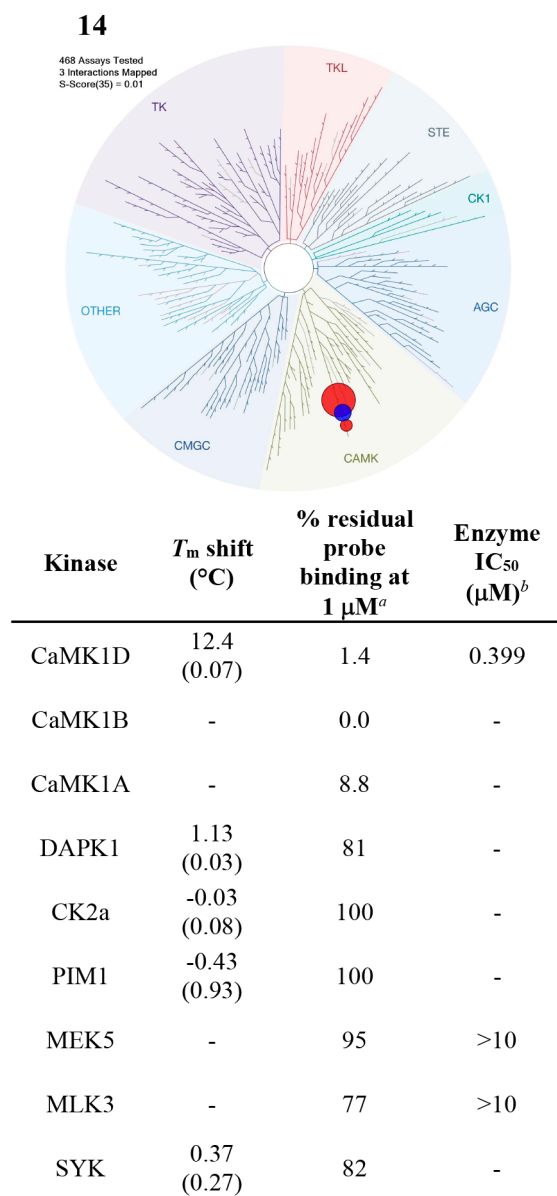


Figure 3. Selectivity data against selected wild-type kinases for compound 14. T_m shift data represents mean of at least $n = 3$ independent experiments with standard deviation in parentheses, see [Supporting Information](#) for experimental details. ^aCompounds tested at Eurofins DiscoverX, $n = 1$. ^bCompounds tested at Reaction Biology, $n = 1$.

revealing slightly higher exposure in DIO mice relative to earlier pharmacokinetic studies ([Figure 5](#)) and no significant changes in exposure on repeat dosing for 14 days at 25 mg/kg. DIO mice treated with a single dose of 25 or 50 mg/kg **18** (in 1:9 DMSO/20% aqueous 2-hydroxypropyl- β -cyclodextrin) 4 h prior to an oral glucose tolerance test (OGTT) show improved glucose control and increased insulin sensitivity relative to vehicle controls ([Figure 9A](#)), with no significant difference in effect between the 25 mg/kg and 50 mg/kg dose groups. Repeat administration of **18** twice daily for 14 days (in 1:9 DMSO/20% aqueous 2-hydroxypropyl- β -cyclodextrin on days 1–6, and 1% methyl cellulose on days 7–14) resulted in reduced baseline glucose and insulin levels, as well as reduced peak glucose levels following OGTT. While there was no effect on glucose AUCB2 in this experiment, the improvement in apparent insulin

sensitivity was maintained, and the overall profile was similar to the positive control liraglutide, which demonstrated a similar profile to that expected based on previous data. Unfortunately repeat dosing of 50 mg/kg **18** was not tolerated due to bloating of the gastrointestinal tract (resulting in change of vehicle in the 25 mg/kg group at day 7); however this was not observed in subsequent tolerability studies with other compounds at significantly higher exposure/free cover. For example, **19** has been dosed at 40 mg/kg once daily (uid; in 50:45:5 PEG400/water/ethanol) for 21 days in NGS mice with no observable adverse effects, suggesting that the GI effects seen with **18** are unlikely to be target related.

CHEMISTRY

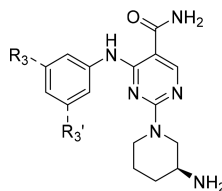
Compounds **1** and **2** are known compounds and were prepared using the previously reported synthesis.¹⁶ Analogues **3–8** were prepared from ethyl 2,4-dichloropyrimidine-5-carboxylate **20** via the 2-HOBt pyrimidine intermediate **21**, which was prepared as previously described,¹⁶ by displacement of the 2-HOBt by the appropriate Boc-protected amine and Boc removal under acidic conditions ([Scheme 1](#)).

To explore the aniline component, the tail was fixed to the (*S*)-3-aminopiperidine and a new synthetic strategy was sought to provide more rapid access to analogues with varied aniline substituents. The commercially available 2,4-dichloropyrimidine-5-carboxamide **22** allows formation of the final products in a typically 3-step process, by sequential displacement using the aniline followed by protected (*S*)-3-aminopiperidine and final acidic deprotection ([Scheme 2](#)). The synthesis can be abbreviated by utilizing excess unprotected (*S*)-3-aminopiperidine directly in the second stage, with the increased nucleophilicity of the cyclic secondary amine resulting in <1% formation of the product resulting from reaction at the primary amine. In general, this approach complicates the purification of the final compounds and as such has not been extensively used but may be useful when introducing acid-sensitive anilines.

The route outlined in [Scheme 2](#) provided ready access to compounds **9–14** by utilizing commercially available anilines in stage 1. Subsequent synthetic effort focused on preparation of anilines designed to develop the emerging SAR in this series. The symmetrical anilines **27** and **28** were initially synthesized by Suzuki reaction on dibromo precursors **23** and **24**; however it was later found that use of the nitro derivatives **25** and **26** results in a slightly cleaner reaction and easier purification, without adding extra steps as the nitro group and carbon–carbon double bonds are reduced in a single stage by heterogeneous hydrogenation ([Scheme 3](#)).

In order to prepare the mixed ^tBu/methylsulfone aniline **34**, the commercially available nitro compound **29** was treated with chlorosulfonic acid in chloroform at reflux to afford the sulfonyl chloride **30**, which was reduced to the thiol **31** with triphenyl phosphine in refluxing toluene. Alkylation of **31** with methyl iodide provided the methyl sulfide **32**, which was oxidized with *m*-CPBA to the corresponding sulfone **33**, before nitro group reduction by heterogeneous hydrogenation to provide aniline **34** ([Scheme 4](#)).

The cyanoisopropyl anilines used in compounds **17** and **18** were prepared from 3,5-dibromoaniline **27** by bis-benzylation to give **35** followed by treatment with potassium 2-cyano-2-methylpropanoate and palladium catalyst³¹ to afford a separable mixture of the symmetrical aniline **36** and partially reacted bromo derivative **37**. Compound **37** was submitted to a second Suzuki coupling to afford intermediate **38**. Debenzylation of **36**

Table 3. Effects of Varying Substitution of Bis-*meta*-Substituted Anilines on Potency and Selectivity

| compd | R ₃ | R ₃ ' | T _m shift (°C) | | | | | | CaMK1D IC ₅₀ (μM) | |
|-------|----------------------|----------------------|---------------------------|-------------|-------------|--------------|-------------|-------------|------------------------------|----------------------------|
| | | | CaMK1D | SYK | DAPK1 | CK2a | ABL | PIM1 | enzyme | cell |
| 15 | <i>i</i> Pr | <i>i</i> Pr | 11.9 (0.15) | 8.20 (0.37) | 4.65 (0.19) | 4.05 (0.07) | 5.95 (0.17) | 0.62 (0.32) | 0.115 (0.051) | 0.285 ^b (0.013) |
| 16 | <i>t</i> Bu | SO ₂ Me | 11.8 (0.25) | 0.87 (0.38) | 3.83 (0.19) | 1.85 (0.16) | 1.09 (0.06) | 0.94 (0.46) | 0.027 (0.005) | 0.028 ^b (0.011) |
| 17 | 2-cyano- <i>i</i> Pr | Ph | 15.9 (0.13) | | 4.8 (0.2) | -0.21 (0.37) | 1.95 (0.02) | 1.11 (0.14) | 0.022 (0.009) | 0.019 ^b (0.001) |
| 18 | 2-cyano- <i>i</i> Pr | 2-cyano- <i>i</i> Pr | 11.5 (0.17) | | 3.46 (0.23) | 0.56 (0.16) | 0.27 (0.16) | 0.81 (0.27) | 0.031 (0.003) | 0.008 (0.002) |

^aAll data represent mean of at least $n = 3$ independent experiments with standard deviation in parentheses, unless otherwise noted. ^b $n = 2$.

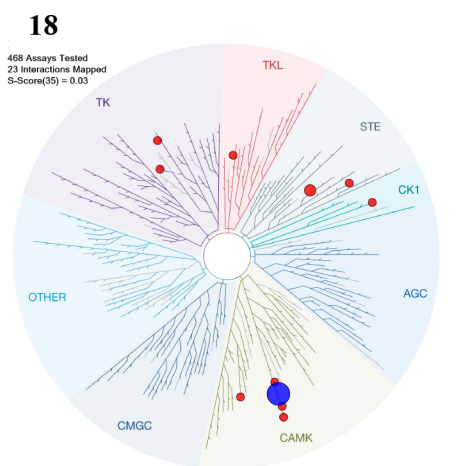


Figure 4. Selectivity data against selected wild-type kinases for compound 18. ^aCompounds tested at Eurofins DiscoverX, $n = 1$. ^bCompounds tested at Reaction Biology, $n = 2$ independent experiments with standard deviation in parentheses, except ^c $n = 1$.

and 39 by heterogeneous hydrogenation provided the anilines 38 and 40 (Scheme 5).

EXPERIMENTAL SECTION

T_m Shift Assays. Thermal melting experiments were carried out using a Stratagene Mx3005p Real Time PCR machine (Agilent Technologies). Proteins were buffered in 10 mM HEPES, pH 7.5, 500 mM NaCl and assayed in a 96-well plate at a final concentration of 2 μM

in a 20 μL volume. Compounds were added at a final concentration of 10 μM (final DMSO concentration was 0.025%). SYPRO Orange (Molecular Probes) was added as a fluorescence probe at a dilution of 1:1000 (v/v). Excitation and emission filters for the SYPRO-Orange dye were set to 465 and 590 nm, respectively. The temperature was raised with a step of 3 °C per minute from 25 to 96 °C, and fluorescence readings were taken at each interval. Experiments were performed in triplicate, and the observed temperature shifts, ΔT_m^{obs} , were recorded as the difference between the transition midpoints of sample and reference wells containing protein without ligand in the same plate and determined by nonlinear least-squares fit, reported in °C as the mean of the values obtained from 3 independent repeats.

CaMK1D ADP GLO Assay. Test compounds were prepared in 100% DMSO, and 12 nL was dispensed to individual wells of a multiwell plate (PerkinElmer, catalog no. 6007290). A reaction mixture containing full length His tagged CaMK1D (Fisher Scientific, PR6770A), calmodulin (Merck, 208694), and autocamtide-2 (Signal-Chem, A15-58) was prepared in assay buffer composed of 50 mM Tris-HCl, pH 7.5, 10 mM MgCl₂, 0.1 CaCl₂ and 2 mM DTT. A 7.88 μL portion of reaction mixture was added to each well to give final assay concentrations: 3 nM CaMK1D, 1 μM calmodulin, and 125 μM autocamtide-2. Plates were centrifuged at 300 rpm for 30 s and incubated for 15 min at 25 °C. The enzyme reaction was initiated by the addition of 4 μL of 30 μM ATP solution to give a final assay concentration of 10 μM. Plates were centrifuged at 300 rpm for 30 s and then incubated at 25 °C for 2 h. ADP-Glo (Promega, catalog no. V9102) was prepared according to manufacturer's instructions and equilibrated to room temperature, shielded from light. Addition of 12 μL of ADP-Glo reagent was made to terminate the kinase reaction and deplete residual ATP. Plates were centrifuged at 300 rpm for 30 s and then incubated at 25 °C for 1 h. Following ATP depletion, 24 μL of ADP-Glo substrate was added to convert ADP to ATP and initiate a luciferase/luciferin chemiluminescent reaction. Plates were centrifuged at 300 rpm for 30 s and then incubated at 25 °C for 30 min, shielded from light. After 30 min, plates were read with the EnVision Multilabel Plate Reader, using Luminescence 700. Compound IC₅₀ was determined using a 4-parameter equation and reported as the geometric mean of the IC₅₀ values obtained from 3 independent repeats.

pCaMK1D Cell Assay. MDA-MB-231 cells were purchased from the ATCC and routinely cultured in DMEM containing 10% FCS and 5 U/mL penicillin/streptomycin (Gibco). MDA-MB-231-HA-CaMK1D cells were established by infecting MDA-MB-231 cells with modified pLVx-HA-CaMK1D lentivirus. Transduced cells were selected in media containing puromycin (2 μg/mL), and expression of CamK1D was verified by Western blotting using rabbit anti-CamK1D mAb ([EPR3536(2)] (ab172618), used at 0.1 mg/mL). Custom made anti-pCamK1D (Ser179, Thr180) polyclonal antibodies were prepared by LifeTein (Hillsborough, NJ, USA), immunizing MEGKGDVM-(pS)(pT)ACGTPGYVA peptide, and verified in a series of Western blotting experiments. MDA-MB-231-HA-CaMK1D cells were cultured in DMEM Glutmax (31966-021, ThermoFisher) containing 10% fetal

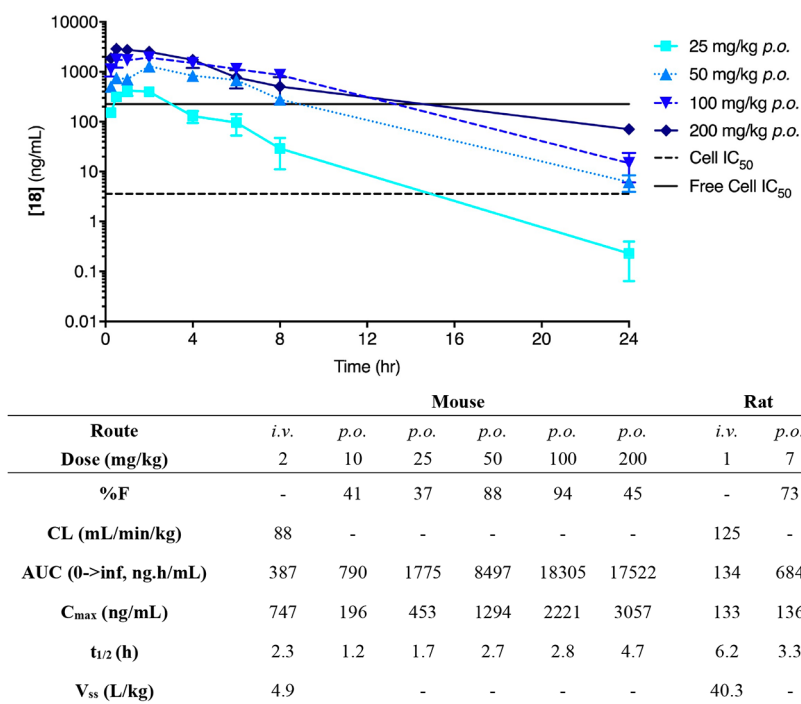


Figure 5. *In vivo* pharmacokinetic profile of **18** in male CD-1 mice (25–40 g) and male Crl:CD Sprague–Dawley rats (250–400 g) dosed in 10% DMSO/90% hydroxypropyl- β -cyclodextrin (20% w/v), $n = 3$ per group. Free cell IC₅₀ was calculated by dividing measured cellular IC₅₀ by free fraction in mouse plasma.

bovine serum (FBS) and 1% penicillin–streptomycin. For the assay, cells were seeded at 1.25×10^5 cells/mL in 6-well plates and maintained at 37 °C in a humidified incubator with 5% CO₂ and 95% air for 48 h. Then, cells were treated with compound for 4 h with a final DMSO concentration of 0.1%; for each compound, an 11-point serial dilution was used and DMSO was included as a control. Media was aspirated, and the cells were washed with PBS. Cells were lysed, supernatants were recovered by centrifugation at 13 000 rpm, protein concentrations were measured, and equal amounts of total protein were separated by SDS-PAGE. Proteins were transferred to PVDF membranes (Bio-Rad), which was followed by blocking for 1 h in 5% milk in TBS-T. Membranes were incubated overnight at 4 °C with primary antibody: anti-pCamK1D (Ser179, Thr180) (1:1000) or total CaMK1D (1:10000, ab172618, Abcam). Membranes were incubated with the corresponding HRP-conjugated secondary antibody (7074S, CST) for 1 h. Specific bands were detected using the enhanced-chemiluminescence reagent (Clarity Western substrate, Bio-Rad) and the ChemiDoc MP Gel Imaging System (Bio-Rad), and % change in pCaMK1D from control was calculated using a ratio of pCaMK1D to total CaMK1D bands. Compound IC₅₀ was determined using a 4-parameter equation and reported as the geometric mean of the IC₅₀ values obtained from 3 independent repeats.

Oral Glucose Tolerance Test after Acute and Chronic, Subacute (14 Day) Dosing. Male C57Bl/6J mice obtained from Charles River UK (Margate, Kent, UK) at 7–8 weeks of age were group housed for 16 weeks ($n = 3$ in each cage) on a normal light/dark cycle (lights on 07:00–19:00 h) with *ad libitum* access to a high fat diet (D12451 diet, 45% kcal as fat, 35% as carbohydrate; Research Diets, New Jersey, USA) and filtered water.

Acute Dosing Study. Animals were allocated to dosing groups (6 mice per group) such that groups were balanced as closely as possible for mean body weight. The day prior to the OGTT, all animals were deprived of food (but not water) beginning approximately 16:45. The following morning, the mice were dosed with vehicle or either 10 mg/kg, 25 mg/kg, or 50 mg/kg **18** formulated in a vehicle of DMSO (10% final volume) and 20% (2-hydroxypropyl)- β -cyclodextrin (90% final volume) by the oral route (beginning at 08:45). Four hours after dosing, a blood sample was taken (B1), and 3 min later glucose was

administered (2 g/kg orally). Further blood samples were taken 10, 30, 60, and 90 min after glucose administration. Between blood sampling, animals were returned to the home cage with free access to water (but not food). Blood samples (approximately 30 μ L) were collected into lithium heparinized tubes (Sarstedt Microvette CB300LH), and plasma was separated by centrifugation to produce a single aliquot of plasma, which was frozen (approximately –80 °C) and subsequently assayed for glucose (in duplicate; Thermoelectron Infinity glucose reagent TR15498) and insulin (single replicate; Alpco mouse ultrasensitive insulin kit 80, INSMSU-E10).

Chronic Dosing Study. Upon completion of the OGTT, all animals were singly housed with food provided as above for 2 weeks prior to the onset of the baseline phase of the chronic study. Upon single housing after the OGTT, mice were placed on a reverse-phase light–dark cycle (lights off 09:30–17:30). Following this period, the animals underwent a 5-day baseline phase where they were dosed twice daily with vehicle at approximately 08:45 and 16:45 each day. Toward the end of the baseline phase mice were reallocated to dosing groups (8 animals per group) such that groups within the study were balanced as closely as possible for body weight, food and water intake, and previous treatment. From day 1 onward, mice were dosed orally twice daily with 25 mg/kg **18** formulated in a vehicle of DMSO (10% final volume) and 20% (2-hydroxypropyl)- β -cyclodextrin (90% final volume) on days 1–6 and 1% methyl cellulose at 5 mL/kg on subsequent days or twice daily orally with vehicle alone or subcutaneously with 0.1 mg/kg liraglutide (Bachem) formulated in pH 7.4 phosphate buffer solution. Oral dosing began at approximately 08:45 and 16:45, with subcutaneous dosing at 08:45 only. Dosing continued until the morning of day 14, when food was removed beginning at approximately 16:45. Approximately 16 h postfast, the animals were moved to a separate room maintained under normal lighting and dosed with vehicle or test compounds in the normal manner to a timed schedule 4 h prior to the administration of the glucose challenge (2.0 g/kg po). Blood samples were taken immediately prior to dosing (B1), immediately prior to glucose administration (B2), and 15, 30, 60, and 90 min after glucose administration. All blood samples (approximately 30 μ L) were taken in lithium heparin-coated tubes (Sarstedt CB300LH) and spun as soon as possible in a centrifuge.

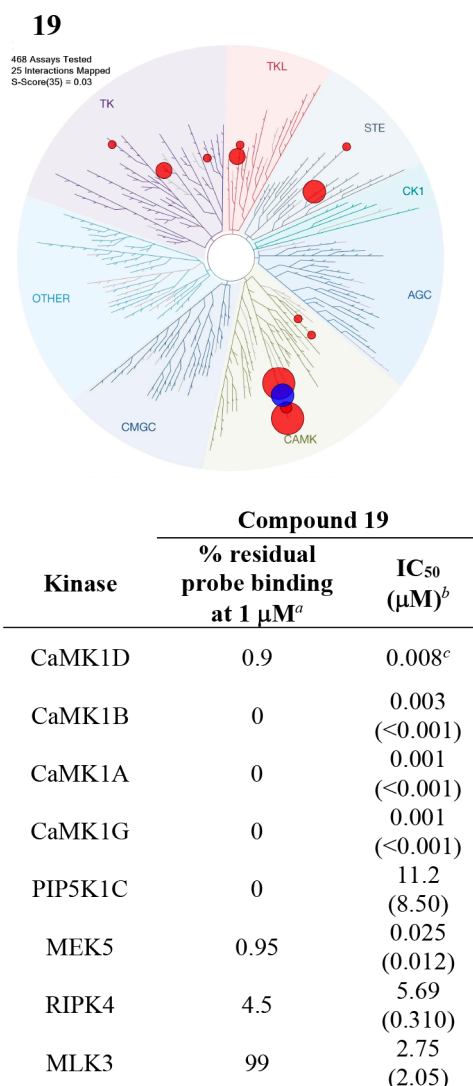


Figure 6. Selectivity data against selected wild-type kinases for compound 19. ^aCompounds tested at Eurofins DiscoverX, $n = 1$. ^bCompounds tested at Reaction Biology data, $n = 2$ independent experiments with standard deviation in parentheses, except ^c $n = 1$.

Plasma samples were stored frozen (approximately $-80\text{ }^\circ\text{C}$) until determination of plasma glucose (in duplicate; ThermoFisher Infinity glucose reagent TR15498) and insulin (single replicate; Alpcos mouse ultrasensitive insulin kit 80, INSMSU-E10). Plasma glucose and insulin data from the OGTTs were analyzed by robust regression with treatment as a factor and bleeding order and day 1 body weight as covariates. AUC for 0 to 60 (following single dose) and 0 to 90 min

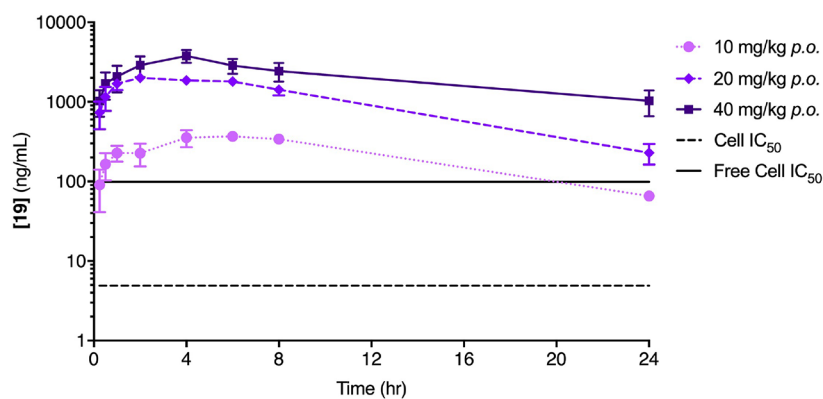
(following repeat dose) was calculated (as total AUC and AUC from baseline) by trapezoidal rule and analyzed by the same methodology. In all cases, this analysis was followed by multiple t test comparisons to determine significant differences in both absolute levels and AUC from the vehicle group.

General Chemistry Experimental Methods. Commercially available and enantiomerically pure *tert*-butyl (*S*)-piperidin-3-ylcarbamate and *tert*-butyl (*R*)-piperidin-3-ylcarbamate were purchased from Carbosynth Ltd. (e.g., FB11271) and used as provided. All other commercially available starting materials, reagents, and solvents were purchased and used without further purification. The reactions were monitored by thin-layer chromatography (60 on aluminum sheets with F254) or by LCMS. LC data was obtained using a Waters ACQUITY UPLC PDA detector scanning between 210 and 400 nm. Mass spectrometry data was acquired using a Waters ACQUITY QDa detector scanning in the positive (ES^+) and negative (ES^-) modes between m/z 100 and 1000. Separation of components was achieved using a Waters ACQUITY UPLC BEH C18 1.7 μm , 2.1 mm \times 50 mm column coupled to a Waters ACQUITY UPLC BEH C18 1.7 μm VanGuard precolumn, 2.1 mm \times 5 mm. Columns were maintained at $40\text{ }^\circ\text{C}$ throughout acquisition. Data was processed using MassLynx V4.1. Values of purity were obtained through analysis of the peak areas in the LC trace between 0.40 and 3.50 min. Purity and identity of all tested compounds were established by a combination of mass spectrometry, HRMS, and NMR spectra as described below. Purification of isolated products was carried out by column chromatography in silica gel (particle size 40–63 μm , Merck) or medium pressure liquid chromatography (MPLC) on a CombiFlash Companion (Teledyne ISCO) with AquaGold prepacked reverse-phase C18 columns. Nuclear magnetic resonance (NMR) spectra were obtained on a Bruker Avance 400 or 500 MHz spectrometer. Chemical shifts (δ) are reported in ppm using the residual signal of the deuterated solvent ($\text{MeOD-}d_4$, CDCl_3 , $\text{DMSO-}d_6$) as internal standard, and coupling constants (J) are reported in Hertz (Hz). The multiplicities are abbreviated as follows: s = singlet, d = doublet, t = triplet, q = quartet, quint = quintet, sext = sextet, sept = septet, m = multiplet, br = broad signal. High-resolution mass spectra were obtained on a Thermo Finigan MAT95XP, magnetic sector mass spectrometer, electron ionization. HPLC method 1: Performed on a Shimadzu UFLCXR system coupled to an Applied Biosystems API2000; column maintained at $40\text{ }^\circ\text{C}$; column, Phenomenex Gemini-NX 3 μm , 110 \AA C18, 50 mm \times 2 mm; total flow rate 0.5 mL/min; UV detection at 220 nm (channel 2) and 254 nm (channel 1); gradient, pre-equilibration run for one min at 5% B, then method run 5–98% solvent B in 2 min, 98% B for 2 min, 98–5% B in 0.5 min then 5% for 1 min; acid method solvent A = 0.1% formic acid in water and solvent B = 0.1% formic acid in MeCN. HPLC method 2: Performed on an Agilent HPLC; column, Waters X-Select C18 2.5 μm , 4.6 mm \times 30 mm, using standard acidic (0.1% formic acid) 4 min method, 5–95% MeCN/water, UV detection at 254 nm. HPLC method 3: Performed on a Waters ACQUITY UPLC with PDA detector scanning between 210 and 400 nm. Mass spectral data was obtained using a Waters ACQUITY QDa detector scanning in the positive (ES^+) and negative (ES^-) modes between m/z 100–650. Samples were passed through a

Table 4. Effects of Introducing 2,6-Di-isopropylpyridine on Potency and Selectivity of Compound 19^a

| compd | T _m shift ($^\circ\text{C}$) | | | | | CaMK1D IC ₅₀ (μM) | |
|-------|---|-------------|------------|-------------|-------------|---|---------------|
| | CaMK1D | DAPK1 | CK2a | ABL | PIM1 | enzyme | cell |
| 19 | 16.0 (0.24) | 5.25 (0.02) | 1.54 (0.2) | 2.34 (0.06) | 0.55 (0.24) | 0.008 (0.001) | 0.011 (0.001) |

^aAll data represent mean of at least $n = 3$ independent experiments with standard deviation in parentheses.



| | Mouse | | | | Rat | | |
|-----------------------------|-------|------|------|-------|-------|------|-------|
| | Route | i.v. | p.o. | p.o. | p.o. | i.v. | p.o. |
| Dose (mg/kg) | | 2 | 10 | 20 | 40 | 2 | 10 |
| F% | | - | 44 | 118 | 100 | - | 67.5 |
| CL (mL/min/kg) | | 13.7 | - | - | - | 36.5 | - |
| AUC (0-inf, ng.hr/mL) | | 2454 | 5408 | 28923 | 49220 | 913 | 3058 |
| C _{max} (ng/mL) | | 503 | 387 | 2015 | 3792 | 391 | 199 |
| t _{1/2} (h) | | 8.3 | 5.9 | 5.9 | 6.2 | 7.7 | 7.0 |
| V _{ss} | | 7.46 | - | - | - | 18.5 | - |
| Kp, uu (@t _{max}) | | - | - | - | - | - | 0.001 |

Figure 7. *In vivo* pharmacokinetic profile of **19** in male CD-1 mice (25–40 g) and male Crl:CD Sprague–Dawley rats (250–400 g) dosed in 10% DMSO/90% hydroxypropyl- β -cyclodextrin (20% w/v), $n = 3$ per group. Free cell IC₅₀ calculated by dividing measured cellular IC₅₀ by free fraction in mouse plasma.

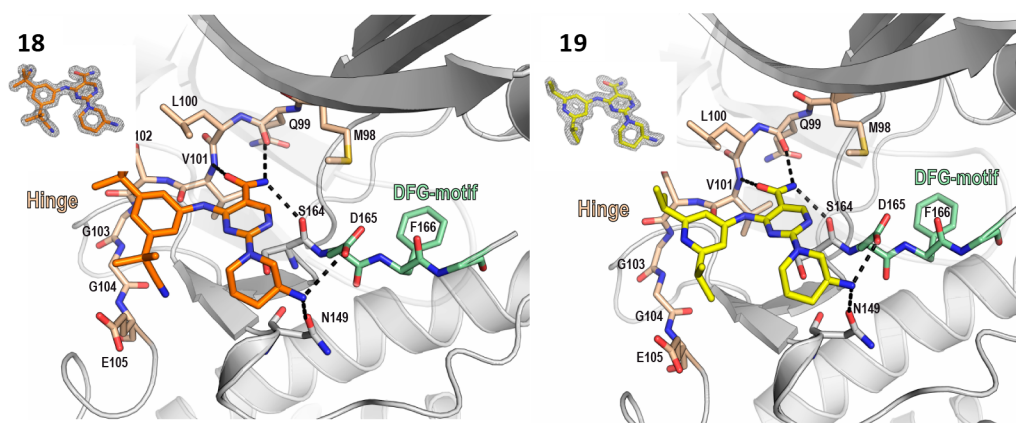


Figure 8. Comparison of the CaMK1D bound structures of compounds **18** (6T29) and **19** (6T28). CaMK1D is shown as gray cartoon representation, the hinge region is highlighted in wheat, and the DFG motif is shown in green color. Important residues and inhibitors are shown in stick representation. For better visibility, the P-Loop has been made transparent. Hydrogen bonds are indicated as black dashed lines. The insets on the upper left of each figure show the electron density of the compounds as $2F_o - F_c$ maps contoured at 1.5σ .

Waters ACQUITY UPLC BEH C18 1.7 μ m, 2.1 mm \times 50 mm column coupled to a Waters ACQUITY UPLC BEH C18 VanGuard precolumn 2.1 mm \times 5 mm. Gradient: Pre-equilibration run for 30 s at 5% B; then method run 5–95% solvent B in 2 min, 95% B for 30 s, 95–5% B in 6 s, then 5% B for 54 s. The column was maintained at 40 $^{\circ}$ C. Acid method: solvent A = 0.1% formic acid in water; solvent B = MeCN. Base method: solvent A = 0.1% ammonium hydroxide in water; solvent B = MeCN. HPLC method 4: Performed on an Agilent HPLC; column Waters X-Bridge C18 2.5 μ m, 4.6 mm \times 30 mm, using standard basic (0.1%

ammonium bicarbonate) 4 min method, 5–95% MeCN/water, UV detection at 254 nm. Compound purity was assessed by HPLC method 1 using both Phenomenex Gemini-NX 3 μ m, 110 \AA C18, 50 mm \times 2 mm and Phenomenex Luna-NX 3 μ m, 110 \AA PFP, 50 mm \times 2 mm columns, with UV detection at 254 nm. All compounds demonstrate purity >95% by both methods, with the exception of **5**, which demonstrates 92.5% purity on the Gemini C-18 column and 96.4% purity on the Luna PFP column.

Table 5. *In Vitro* Pharmacokinetic and Toxicology Profile of 18 and 19

| | 18 | 19 |
|---|-------------------|------------------|
| LogD | 2.3 | 2.6 |
| solubility (μM) | 52 | >200 |
| mouse/rat/human MICs ($\mu\text{L}\cdot\text{min}^{-1}\cdot\text{mg}^{-1}$) | 15/<1/13 | 6/3/7 |
| mouse/rat/human Heps ($\mu\text{L}\cdot\text{min}^{-1}$ per 10^6 cells) | 13/11/ <i>b</i> | 14/ <i>b</i> /19 |
| mouse/rat/human PPB (% bound) | 98.4/94/ <i>b</i> | 94/92/89 |
| CaCo2 P_{app} (A–B $\times 10^{-6}$ cm/s)/efflux ratio | 1.1/13.4 | 0.4/7.9 |
| CYP450 2C9/2C19 IC ₅₀ (μM) ^a | 6/1 | 6/10 |
| Ionworks hERG IC ₅₀ (μM)/ratio to cell IC ₅₀ | 7.1/284 | 3.7/336 |

^aCYP450 1A2, 2D6, and 3A45 IC₅₀ > 20 μM for all compounds. ^bNot determined.

2-((2-Aminoethyl)amino)-4-((3-(trifluoromethyl)phenyl)amino)pyrimidine-5-carboxamide hydrochloride (1). Compound prepared following a reported method.¹⁶ ¹H NMR (400 MHz, DMSO-*d*₆) δ 12.34 (s, 1H), 8.91 (s, 1H), 8.61 (br s, 2H), 8.32 (br s, 3H), 8.13 (s, 1H), 7.90 (d, *J* = 8.1 Hz, 1H), 7.70 (app. t, *J* = 8.1 Hz, 1H), 7.55 (d, *J* = 8.1 Hz, 1H), 3.64 (app. q, *J* = 5.6 Hz, 2H), 3.01 (app. q, *J* = 5.6 Hz, 2H); LC-MS *m/z* (ES⁺) (M + H)⁺ 341.2; *t*_R = 1.98 min. HPLC method 1. HRMS (ES-TOF): *m/z* calcd for C₁₄H₁₆F₃N₆O 341.1332, found 341.1346 [M + H]⁺.

2-((2-Aminoethyl)amino)-*N*-methyl-4-((3-(trifluoromethyl)phenyl)amino)pyrimidine-5-carboxamide (2). Compound prepared following a reported method.¹⁶ ¹H NMR (DMSO-*d*₆) δ 12.21 (s, 1H), 9.30 (d, *J* = 3.9 Hz, 1H), 8.88 (s, 1H), 8.66 (app. t, *J* = 5.2 Hz, 1H), 8.26 (br s, 3H), 8.14 (s, 1H), 7.91 (d, *J* = 7.9 Hz, 1H), 7.70 (app. t, *J* = 7.9 Hz, 1H), 7.56 (d, *J* = 7.8 Hz, 1H), 3.64 (app. q, *J* = 4.8 Hz, 2H), 3.02 (app. q, *J* = 4.8 Hz, 2H), 2.78 (d, *J* = 4.4 Hz, 3H); LC-MS *m/z* (ES⁺) (M

+ H)⁺ 355.2; *t*_R = 1.99 min. HPLC method 1. HRMS (ES-TOF): *m/z* calcd for C₁₅H₁₇F₃N₆O_{Na} 377.1308, found 377.1301 [M + Na]⁺.

2-((2-Aminoethyl)(methylamino)-4-((3-(trifluoromethyl)phenyl)amino)pyrimidine-5-carboxamide Hydrochloride (3). To a suspension of 2-((1*H*-benzo[*d*][1,2,3]triazol-1-yl)oxy)-4-((3-(trifluoromethyl)phenyl)amino)pyrimidine-5-carboxamide **21** (0.11 g, 0.25 mmol), prepared following a reported method,¹⁶ in THF (2 mL) and DMF (1 mL) was added *N*-*boc*-2-methylamino-ethylamine (50 mg, 0.28 mmol), and the mixture was stirred for 30 min at room temperature. The mixture was diluted with water and extracted with AcOEt. The organic layer was dried over anhydrous Na₂SO₄ and concentrated under reduced pressure. *m/z* (ES⁺) (M + H)⁺ 455.0; *t*_R = 2.74 min. HPLC method 1. The crude was dissolved in CH₂Cl₂ (2 mL), and 4 N HCl in dioxane (5 mL) was added. The suspension was stirred at RT for 1 h (completion monitored by HPLC). The suspension was concentrated, and Et₂O was added to induce precipitation. The resulting white solid was centrifuged, washed again with Et₂O, and dried under vacuum affording the titled compound (50 mg, 81%). ¹H NMR (400 MHz, MeOD-*d*₄) δ 8.61 (s, 1H), 8.09 (br s, 1H), 7.78 (d, *J* = 7.6 Hz, 1H), 7.66 (app. t, *J* = 7.8 Hz, 1H), 7.57 (d, *J* = 7.6 Hz, 1H), 3.99 (t, *J* = 5.7 Hz, 2H), 3.36 (s, 3H), 3.26 (br s, 2H); LC-MS *m/z* (ES⁺) (M + H)⁺ 355.2; *t*_R = 2.09 min. HPLC method 1. HRMS (ES-TOF): *m/z* calcd for C₁₅H₁₈F₃N₆O 355.1489, found 355.1503 [M + H]⁺.

2-(Methyl(2-(methylamino)ethyl)amino)-4-((3-(trifluoromethyl)phenyl)amino)pyrimidine-5-carboxamide Hydrochloride (4). Prepared in analogous manner to **3** using *N*-*boc*-2,4-dimethylamino-ethylamine. ¹H NMR (400 MHz, MeOD-*d*₄) δ 8.62 (s, 1H), 8.06 (br s, 1H), 7.82 (d, *J* = 7.8 Hz, 1H), 7.69 (app. t, *J* = 7.8 Hz, 1H), 7.60 (br d, *J* = 7.1 Hz, 1H), 4.05 (t, *J* = 5.6 Hz, 2H), 3.38 (s, 3H), 3.32 (br s, 2H), 2.59 (br s, 3H); LC-MS *m/z* (ES⁺) (M + H)⁺ 369.2; *t*_R = 2.12 min. HPLC method 1. HRMS (ES-TOF): *m/z* calcd for C₁₆H₂₀F₃N₆O 369.1645, found 369.1659 [M + H]⁺.

2-((2-(Dimethylamino)ethyl)(methylamino)-4-((3-(trifluoromethyl)phenyl)amino)pyrimidine-5-carboxamide

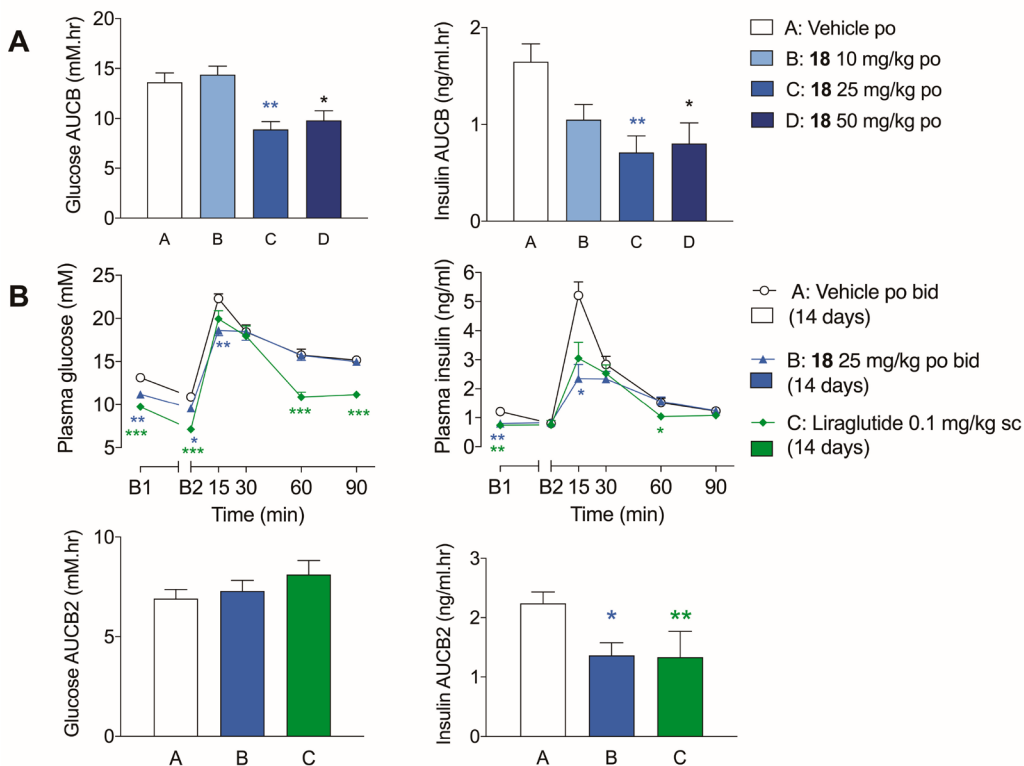
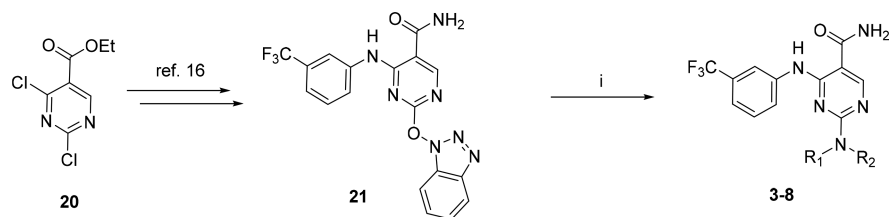
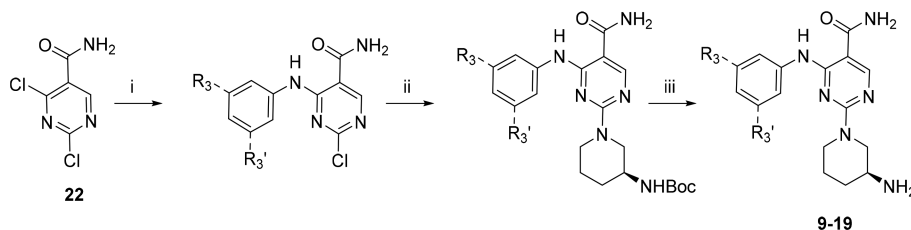


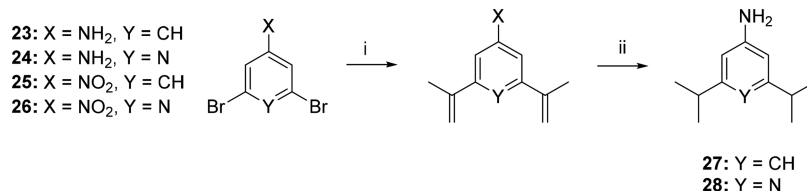
Figure 9. *In vivo* activity of compound **18** following oral glucose tolerance test (OGTT) in diet induced obesity mouse model (male C57Bl/6J mice) following (A) single dose 4 h prior to OGTT ($n = 6$ per group) and (B) 14 day repeat dosing ($n = 8$ per group). Significant differences (from vehicle), determined by multiple *t* test comparisons, are denoted by * $p < 0.05$, ** $p < 0.01$, and *** $p < 0.001$.

Scheme 1. Synthetic Route to Compounds 3–8^a

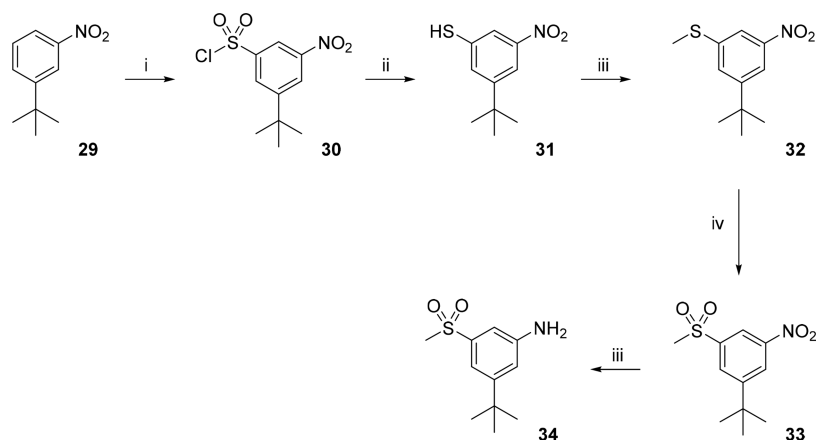
^aReagents and conditions: (i) *N*-Boc-diamine, THF/DMF, RT, 30 min; then DCM, 4 N HCl in dioxane, RT, 1 h, 81%.

Scheme 2. General Synthetic Route to Compounds 9–19^a

^aReagents and conditions: (i) aniline, *i*Pr₂NEt, MeCN or dioxane, reflux, 16 h; (ii) (*S*)-*tert*-butyl piperidin-3-ylcarbamate, DIPEA, solvent, RT, 2–16 h; (iii) TFA/DCM or 4 N HCl in dioxane, RT, 1 h, 10–73% over 3 steps.

Scheme 3. Synthesis of Di-alkyl (Hetero)anilines 27 and 28, Used in Compounds 15 and 19^a

^aReagents and conditions: (i) (4,4,5,5-tetramethyl-1,3,2-dioxaborolan-2-yl)isoprene, NaHCO₃, Pd(dppf)Cl₂ or Pd(PPh₃)₄, 1,4-dioxane, water, 90 °C, 4–16 h, 54–83%; (ii) H₂, Pd/C, MeOH, RT, 2–16 h, 75–98%.

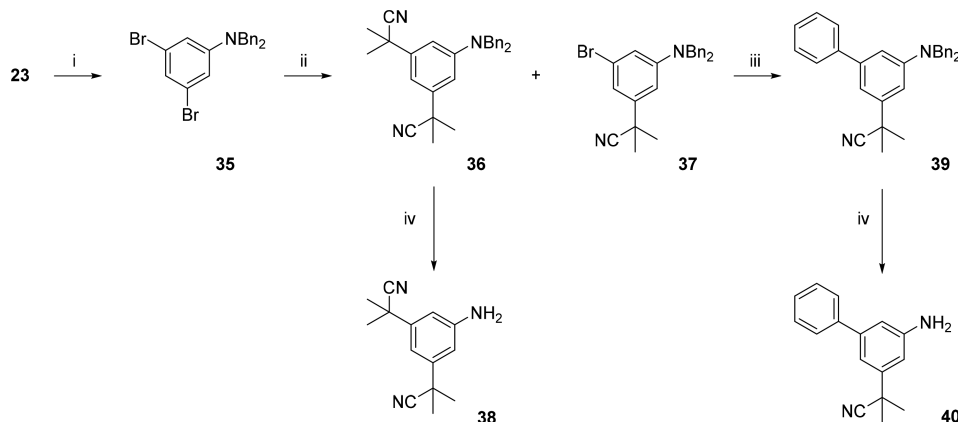
Scheme 4. Synthesis of Aniline 34, Used in Compound 16^a

^aReagents and conditions: (i) chlorosulfonic acid, CHCl₃, reflux, 48 h, 85%; (ii) P(Ph)₃, toluene, RT, 10 min, 72%; (iii) NaOH, MeI, EtOH, RT, 16 h, 98%; (iv) *m*-CPBA, DCM, 0 °C to RT, 2 h, 73%; (v) H₂ (5 atm), Pd/C, MeOH, 16 h, 76%.

Hydrochloride (5). Prepared in analogous manner to 3 with *N*-boc-2,4,4-trimethylamino-ethylamine. ¹H NMR (400 MHz, MeOD-*d*₄) δ 8.61 (s, 1H), 7.96 (br s, 1H), 7.82 (d, *J* = 7.1 Hz, 1H), 7.70 (app. t, *J* = 7.4 Hz, 1H), 7.63 (br s, 1H), 4.09 (app. t, *J* = 5.4 Hz, 2H), 3.42 (br s, 2H), 3.33 (s, 3H), 2.68 (br s, 6H); LC-MS *m/z* (ES⁺) (*M* + H)⁺ 383.2; *t*_R = 2.12 min. HPLC method 1. HRMS (ES-TOF): *m/z* calcd for C₁₇H₂₂F₃N₆O 383.1802, found 383.1824 [*M* + H]⁺.

(rac)-2-(3-Aminopiperidin-1-yl)-4-((3-(trifluoromethyl)phenyl)amino)pyrimidine-5-carboxamide Hydrochloride (6).

Prepared in analogous manner to 3 using (±)*tert*-butyl-piperidin-3-ylcarbamate. ¹H NMR (400 MHz, MeOD-*d*₄) δ 8.60 (s, 1H), 8.10 (br s, 1H), 7.81 (br d, *J* = 7.1 Hz, 1H), 7.67 (t, *J* = 7.8 Hz, 1H), 7.56 (d, *J* = 7.8 Hz, 1H), 4.35 (dd, *J* = 13.5, 3.7 Hz, 1H), 4.06 (br s, 1H), 3.73 (dd, *J* = 13.5, 8.4 Hz, 1H), 3.64–3.57 (m, 1H), 3.54–3.48 (m, 1H), 2.24–2.16 (m, 1H), 2.02–1.94 (m, 1H), 1.88–1.75 (m, 2H); LC-MS *m/z* (ES⁺) (*M* + H)⁺ 381.4; *t*_R = 2.14 min. HPLC method 1. HRMS (ES-TOF): *m/z* calcd for C₁₇H₂₀F₃N₆O 381.1645, found 381.1662 [*M* + H]⁺.

Scheme 5. Synthesis of 2-Cyanoisopropyl Substituted Anilines Used in Compounds 17 and 18^a

^aReagents and conditions: (i) Benzyl bromide, K₂CO₃, MeCN, reflux, 24 h, 73%; (ii) potassium 2-cyano-2-methylpropanoate, mesitylene, Xantphos, Pd₂(allyl)₂Cl₂, 140 °C, 24 h, 36= 53%, 37= 20%; (iii) 4,4,5,5-tetramethyl-2-phenyl-1,3,2-dioxaborolane, Pd(PPh₃)₂Cl₂, K₂CO₃, dioxane:water, 100 °C, 1 h, 74%; (iv) H₂, Pd/C, MeOH:DCM, 18 h, 88–98%.

(R)-2-(3-Aminopiperidin-1-yl)-4-((3-(trifluoromethyl)phenyl)amino)pyrimidine-5-carboxamide Hydrochloride (7). Prepared in analogous manner to 3 using *tert*-butyl (*R*)-piperidin-3-ylcarbamate. ¹H NMR (400 MHz, MeOD-*d*₄) δ 8.60 (s, 1H), 8.10 (br s, 1H), 7.81 (br d, *J* = 7.1 Hz, 1H), 7.67 (t, *J* = 7.8 Hz, 1H), 7.56 (d, *J* = 7.8 Hz, 1H), 4.35 (dd, *J* = 13.5, 3.7 Hz, 1H), 4.06 (br s, 1H), 3.73 (dd, *J* = 13.5, 8.4 Hz, 1H), 3.64–3.57 (m, 1H), 3.54–3.48 (m, 1H), 2.24–2.16 (m, 1H), 2.02–1.94 (m, 1H), 1.88–1.75 (m, 2H); LC-MS *m/z* (ES⁺) (M + H)⁺ 381.4; *t*_R = 2.14 min. HPLC method 1. HRMS (ES-TOF): *m/z* calcd for C₁₇H₂₀F₃N₆O 381.1645, found 381.1655 [M + H]⁺.

(S)-2-(3-Aminopiperidin-1-yl)-4-((3-(trifluoromethyl)phenyl)amino)pyrimidine-5-carboxamide Hydrochloride (8). Prepared in analogous manner to 3 using *tert*-butyl (*S*)-piperidin-3-ylcarbamate. ¹H NMR (400 MHz, MeOD-*d*₄) δ 8.60 (s, 1H), 8.10 (br s, 1H), 7.81 (br d, *J* = 7.1 Hz, 1H), 7.67 (t, *J* = 7.8 Hz, 1H), 7.56 (d, *J* = 7.8 Hz, 1H), 4.35 (dd, *J* = 13.5, 3.7 Hz, 1H), 4.06 (br s, 1H), 3.73 (dd, *J* = 13.5, 8.4 Hz, 1H), 3.64–3.57 (m, 1H), 3.54–3.48 (m, 1H), 2.24–2.16 (m, 1H), 2.02–1.94 (m, 1H), 1.88–1.75 (m, 2H); LC-MS *m/z* (ES⁺) (M + H)⁺ 381.0; *t*_R = 2.15 min. HPLC method 1. HRMS (ES-TOF): *m/z* calcd for C₁₇H₂₀F₃N₆O 381.1645, found 381.1655 [M + H]⁺.

(S)-2-(3-Aminopiperidin-1-yl)-4-((4-(trifluoromethyl)phenyl)amino)pyrimidine-5-carboxamide Hydrochloride (9). 3,5-Bis(trifluoromethyl)aniline (85 mg, 0.37 mmol) was added to a solution of 2,4-dichloropyrimidine-5-carboxamide 22 (75 mg, 0.39 mmol) and DIPEA (0.17 mL, 0.98 mmol) in dioxane (5 mL) and stirred at 80 °C for 16 h. The reaction was concentrated under reduced pressure (38 mg, 20%). LC-MS *m/z* (ES⁺) (M + H)⁺ 385.0; *t*_R = 2.44 min. HPLC method 2.

(*S*)-*tert*-Butyl piperidin-3-ylcarbamate (62 mg, 0.23 mmol) was added to a solution of 4-((3,5-bis(trifluoromethyl)phenyl)amino)-2-chloropyrimidine-5-carboxamide (38 mg, 0.10 mmol) and TEA (69 μL, 0.49 mmol) in dioxane (10 mL). The reaction was stirred at RT for 16 h. The mixture was diluted with Et₂O (10 mL), filtered, and washed with CH₂Cl₂/MeOH/Et₂O (9:1:9 mL). No further purification was required (20 mg, 19% yield). LC-MS *m/z* (ES⁺) (M + H)⁺ 549.0; *t*_R = 2.75 min. HPLC method 2.

(*S*)-*tert*-Butyl (1-(4-((3,5-bis(trifluoromethyl)phenyl)amino)-5-carbamoylpyrimidin-2-yl)piperidin-3-yl)carbamate (20 mg, 0.04 mmol) was treated with TFA (0.10 mL, 1.08 mmol) in CH₂Cl₂ (1 mL). The reactions were stirred for 2 h and concentrated under reduced pressure. The residues were diluted in MeOH (0.20 mL) and loaded onto a SCX cartridge, washing with MeOH (3 column volumes) and eluting with 1% NH₃ MeOH (3 column volumes). The ammoniacal MeOH was removed under reduced pressure to give the product (12 mg, 16% yield over 3 steps). ¹H NMR (400 MHz, MeOD-*d*₄) δ 8.63 (s, 1H), 8.41–8.31 (m, 2H), 7.60 (s, 1H), 4.67–4.60 (m, 1H), 4.50–4.43 (m, 1H), 3.24–3.18 (m, 1H), 3.03 (dd, *J* = 12.7, 9.4 Hz, 1H), 2.90–2.84 (m, 1H), 2.12–2.04 (m, 1H), 1.91–1.83 (m, 1H), 1.68–1.43 (m,

2H). LC-MS *m/z* (ES⁺) (M + H)⁺ 449.0; *t*_R = 1.59 min. HPLC method 2. HRMS (ES-TOF): *m/z* calcd for C₁₈H₁₉F₆N₆O 449.1519, found 449.1538 [M + H]⁺.

(S)-2-(3-Aminopiperidin-1-yl)-4-((3-(*tert*-butyl)phenyl)amino)pyrimidine-5-carboxamide Hydrochloride (10). Prepared in analogous manner to 9 using 3-*tert*-butyl-aniline. Compound isolated as HCl salt. ¹H NMR (400 MHz, MeOD-*d*₄) δ 8.54 (s, 1H), 7.72 (s, 1H), 7.41 (d, *J* = 7.8 Hz, 1H), 7.28 (t, *J* = 7.9 Hz, 1H), 7.14 (dd, *J* = 7.8, 2.0 Hz, 1H), 4.62 (dd, *J* = 12.6, 3.9 Hz, 1H), 4.53 (d, *J* = 13.2 Hz, 1H), 3.18–3.12 (m, 1H), 2.96 (dd, *J* = 12.7, 9.4 Hz, 1H), 2.85–2.78 (m, 1H), 2.07–1.99 (m, 1H), 1.84–1.77 (m, 1H), 1.63–1.39 (m, 2H), 1.36 (s, 9H); LC-MS *m/z* (ES⁺) (M + H)⁺ 369; *t*_R = 2.01 min. HPLC method 2. HRMS (ES-TOF): *m/z* calcd for C₂₀H₂₉N₆O 369.2397, found 369.2412 [M + H]⁺.

(S)-2-(3-Aminopiperidin-1-yl)-4-((3-(methylsulfonyl)phenyl)amino)pyrimidine-5-carboxamide (11). Prepared in analogous manner to 9 using 3-methylsulfonyl-aniline. ¹H NMR (400 MHz, MeOD-*d*₄) δ 9.08 (s, 1H), 8.61 (s, 1H), 7.67–7.55 (m, 2H), 7.49 (s, 1H), 4.78 (s, 1H), 4.62 (s, 1H), 3.16–3.10 (m, 4H), 2.99–2.92 (m, 2H), 2.09 (br s, 1H), 1.89–1.86 (m, 1H), 1.65–1.59 (m, 1H), 1.53–1.44 (m, 1H); LC-MS *m/z* (ES⁺) (M + H)⁺ 391; *t*_R = 1.30 min. HPLC method 2. HRMS (ES-TOF): *m/z* calcd for C₁₇H₂₃N₆O₃S 391.1547, found 391.1554 [M + H]⁺.

(S)-4-([1,1'-Biphenyl]-3-ylamino)-2-(3-aminopiperidin-1-yl)pyrimidine-5-carboxamide Hydrochloride (12). Prepared in analogous manner to 9 using 3-amino-1,1'-biphenyl. Compound isolated as HCl salt. ¹H NMR (400 MHz, MeOD-*d*₄) δ 8.55 (s, 1H), 7.83 (br s, 1H), 7.64–7.61 (m, 3H), 7.56–7.51 (m, 2H), 7.46 (t, *J* = 7.6 Hz, 2H), 7.39–7.35 (m, 1H), 4.34 (dd, *J* = 13.8, 3.5 Hz, 1H), 4.04 (br s, 1H), 3.78–3.70 (m, 1H), 3.63–3.54 (m, 1H), 3.54–3.47 (m, 2H), 2.23–2.16 (m, 1H), 1.99–1.89 (m, 1H), 1.89–1.73 (m, 2H); LC-MS *m/z* (ES⁺) (M + H)⁺ 389.1; *t*_R = 2.25 min. HPLC method 1. HRMS (ES-TOF): *m/z* calcd for C₂₂H₂₅N₆O 389.2084, found 389.2101 [M + H]⁺.

(S)-2-(3-Aminopiperidin-1-yl)-4-((3-(2-cyanopropan-2-yl)phenyl)amino)pyrimidine-5-carboxamide (13). Prepared in analogous manner to 9 using 2-(3-aminophenyl)-2-methylpropanenitrile. ¹H NMR (400 MHz, MeOD-*d*₄) δ 8.56 (s, 1H), 8.08 (app. t, *J* = 2.0 Hz, 1H), 7.47–7.36 (m, 2H), 7.21 (ddd, *J* = 7.4, 2.0, 1.3 Hz, 1H), 4.67–4.60 (m, 1H), 4.54 (d, *J* = 13.2 Hz, 1H), 3.19–3.09 (m, 1H), 2.96 (dd, *J* = 12.7, 9.4 Hz, 1H), 2.81–2.79 (m, 1H), 2.03 (br s, 1H), 1.84 (br s, 1H), 1.77 (s, 6H), 1.64–1.52 (m, 1H), 1.49–1.36 (m, 1H); LC-MS *m/z* (ES⁺) (M + H)⁺ 380.0; *t*_R = 1.66 min. HPLC method 2. HRMS (ES-TOF): *m/z* calcd for C₂₀H₂₃N₇ONa 402.2013, found 402.2016 [M + Na]⁺.

(S)-2-(3-Aminopiperidin-1-yl)-4-((3,5-di-*tert*-butylphenyl)amino)pyrimidine-5-carboxamide (14). Prepared in analogous manner to 9 using 3,5-di-*tert*-butyl-aniline. ¹H NMR (400 MHz,

isohexane) to afford 2,6-di(prop-1-en-2-yl)pyridin-4-amine (0.20 g, 54%); LC-MS m/z (M + H)⁺ (ES⁺) 175.2; t_R = 0.62 min. HPLC method 2.

Step 2: 2,6-Diisopropylpyridin-4-amine (28). A solution of 2,6-di(prop-1-en-2-yl)pyridin-4-amine (0.20 g, 1.15 mmol) in methanol (4 mL) was hydrogenated in an H-Cube (10% Pd/C, 30 mm × 4 mm, full hydrogen, 40 °C, 1 mL/min) and concentrated under vacuum to afford 2,6-diisopropylpyridin-4-amine (0.15 g, 75%). LC-MS m/z (M + H)⁺ (ES⁺) 179.2; t_R = 1.13 min. HPLC method 4.

Step 3: (S)-2-(3-Aminopiperidin-1-yl)-4-((2,6-diisopropylpyridin-4-yl)amino)pyrimidine-5-carboxamide (19). To a stirred solution of 2,4-dichloropyrimidine-5-carboxamide (0.97 g, 5.02 mmol) in 1,4-dioxane (20 mL) was added 2,6-diisopropylpyridin-4-amine **38** (0.69 g, 3.86 mmol) and DIPEA (1.35 mL, 7.73 mmol). The reaction was heated to 110 °C and stirred for 7 h. The mixture was allowed to cool and concentrated under vacuum. The crude product was purified by chromatography on silica gel (0–2% (0.7 M ammonia/MeOH)/CH₂Cl₂) to afford 2-chloro-4-((2,6-diisopropylpyridin-4-yl)amino)pyrimidine-5-carboxamide (0.91 g, 67%). ¹H NMR (500 MHz, DMSO-*d*₆) δ 11.66 (s, 1H), 8.86 (s, 1H), 8.50 (s, 1H), 8.04 (s, 1H), 7.40 (s, 2H), 2.95 (sept, 2H, *J* = 6.9 Hz), 1.24 (d, 12H, *J* = 6.9 Hz); LC-MS m/z (M + H)⁺ (ES⁺) 334.2; t_R = 2.26 min. HPLC method 4.

To a stirred solution of 2-chloro-4-((2,6-diisopropylpyridin-4-yl)amino)pyrimidine-5-carboxamide (0.91 g, 2.70 mmol) in 1,4-dioxane (20 mL) was added (S)-*tert*-butyl piperidin-3-ylcarbamate (0.57 g, 2.83 mmol) and DIPEA (0.49 mL, 2.83 mmol). The reaction was heated to 90 °C and stirred for 30 min, then allowed to cool and concentrated under vacuum. The crude product was purified by chromatography on silica gel (0–2% (0.7 M ammonia/MeOH)/CH₂Cl₂) to afford (S)-*tert*-butyl (1-(5-carbamoyl-4-((2,6-diisopropylpyridin-4-yl)amino)pyrimidin-2-yl)piperidin-3-yl)carbamate (1.19 g, 88%). LC-MS m/z (M + H)⁺ (ES⁺) 498.5; t_R = 2.49 min. HPLC method 4.

To a stirred solution of (S)-*tert*-butyl (1-(5-carbamoyl-4-((2,6-diisopropylpyridin-4-yl)amino)pyrimidin-2-yl)piperidin-3-yl)carbamate (1.19 g, 2.391 mmol) in 1,4-dioxane (10 mL) was added 4 M hydrochloric acid in dioxane (11.96 mL, 47.8 mmol), and the reaction was stirred at RT for 4 h. The reaction mixture was then concentrated under vacuum. The residue was diluted in MeOH (0.20 mL) and loaded onto a SCX cartridge, washing with MeOH (3 column volumes) and eluting with 1% NH₃ MeOH (3 column volumes). The ammoniacal MeOH was removed under reduced pressure to give the title compound as a white solid (0.85 g, 78%). Mp 225–226 °C; ¹H NMR (500 MHz, MeOD-*d*₄) δ 8.59 (s, 1H), 7.44 (s, 2H), 4.63 (dd, *J* = 12.7, 4.0 Hz, 1H), 4.58–4.50 (m, 1H), 3.22 (ddd, *J* = 13.6, 10.8, 3.2 Hz, 1H), 3.09–2.95 (m, 3H), 2.88–2.77 (m, 1H), 2.08–2.00 (m, 1H), 1.88–1.78 (m, 1H), 1.65–1.52 (m, 1H), 1.51–1.40 (m, 1H), 1.30 (dd, *J* = 7.0, 2.7 Hz, 12H); ¹³C NMR (126 MHz, methanol-*d*₄) δ 170.3, 167.3, 161.0, 159.8, 158.2, 147.7, 108.0, 98.5, 51.0, 44.2, 35.9, 32.5, 23.3, 21.8; LC-MS m/z (M + H)⁺ (ES⁺) 398.3; t_R = 1.79 min. HPLC method 4. HRMS (ES-TOF): m/z calcd for C₂₁H₃₁N₇O₄Na 420.2482, found 420.2473 [M + Na]⁺.

CONCLUSION

We have identified highly potent and selective *in vitro* and *in vivo* probes of CaMK1 kinases through a structure-based design approach. These probes should be of utility to researchers working on CaMK1 biology *in vitro* or who wish to investigate the effects of targeting the peripheral function of CaMK1 enzymes.

ASSOCIATED CONTENT

Supporting Information

The Supporting Information is available free of charge at <https://pubs.acs.org/doi/10.1021/acs.jmedchem.9b01803>.

Molecular SMILES strings and *in vitro* results including number of replicates and standard deviation values (CSV) HPLC traces for **1–19** (PDF)

Experimental data from X-ray crystal structures, experimental details for DIO mouse OGTT study, full Eurofins Discover X profiles, and NMR spectra of **18** and **19** (PDF)

Structure of compound **8** bound to CaMK1D (PDB)

Structure of compound **18** bound to CaMK1D (PDB)

Structure of compound **19** bound to CaMK1D (PDB)

Accession Codes

X-ray coordinates and structures factors have been deposited in the Protein Data Bank under the following accession codes: compound **8**, PDB 6T6F; compound **18**, PDB 6T28; compound **19**, PDB 6T29. Authors will release the atomic coordinates upon article publication.

AUTHOR INFORMATION

Corresponding Author

Sam Butterworth – Division of Pharmacy and Optometry, School of Health Sciences, Manchester Academic Health Sciences Centre, University of Manchester, Manchester M13 9PL, U.K.;

orcid.org/0000-0002-6549-3753;

Email: sam.butterworth@manchester.ac.uk

Authors

Christophe Fromont – Centre for Biomolecular Sciences and School of Pharmacy, University of Nottingham, Nottingham NG7 2RD, U.K.

Alessio Atzori – Centre for Biomolecular Sciences and School of Pharmacy, University of Nottingham, Nottingham NG7 2RD, U.K.

Divneet Kaur – Centre for Biomolecular Sciences and School of Pharmacy, University of Nottingham, Nottingham NG7 2RD, U.K.

Lubna Hashmi – Centre for Biomolecular Sciences and School of Pharmacy, University of Nottingham, Nottingham NG7 2RD, U.K.

Graziella Greco – School of Pharmacy, College of Medical and Dental Sciences, University of Birmingham, Edgbaston B15 2TT, U.K.

Alejandro Cabanillas – School of Pharmacy, College of Medical and Dental Sciences, University of Birmingham, Edgbaston B15 2TT, U.K.

Huy Van Nguyen – School of Pharmacy, College of Medical and Dental Sciences, University of Birmingham, Edgbaston B15 2TT, U.K.; orcid.org/0000-0002-3985-1510

D. Heulyn Jones – Division of Pharmacy and Optometry, School of Health Sciences, Manchester Academic Health Sciences Centre, University of Manchester, Manchester M13 9PL, U.K.

Miguel Garzón – Division of Pharmacy and Optometry, School of Health Sciences, Manchester Academic Health Sciences Centre, University of Manchester, Manchester M13 9PL, U.K.

Ana Varela – Division of Pharmacy and Optometry, School of Health Sciences, Manchester Academic Health Sciences Centre, University of Manchester, Manchester M13 9PL, U.K.

Brett Stevenson – Signature Discovery, Nottingham NG1 1GF, U.K.

Greg P. Iacobini – Signature Discovery, Nottingham NG1 1GF, U.K.

Marc Lenoir – Institute of Cancer and Genomic Sciences, University of Birmingham, Birmingham B15 2TT, U.K.

Sundaresan Rajesh – Institute of Cancer and Genomic Sciences, University of Birmingham, Birmingham B15 2TT, U.K.

Clare Box – Institute of Cancer and Genomic Sciences, University of Birmingham, Birmingham B15 2TT, U.K.

Jitendra Kumar – Department of Biochemistry, University of Alberta, Edmonton, Alberta T6G 2H7, Canada

Paige Grant – Department of Biochemistry, University of Alberta, Edmonton, Alberta T6G 2H7, Canada

Vera Novitskaya – Institute of Cancer and Genomic Sciences, University of Birmingham, Birmingham B15 2TT, U.K.

Juliet Morgan – Sygnature Discovery, Nottingham NG1 1GF, U.K.

Fiona J. Sorrell – Structural Genomics Consortium and Target Discovery Institute, Nuffield Department of Clinical Medicine, University of Oxford, Oxford OX3 7DQ, U.K.

Clara Redondo – Structural Genomics Consortium and Target Discovery Institute, Nuffield Department of Clinical Medicine, University of Oxford, Oxford OX3 7DQ, U.K.

Andreas Kramer – Structural Genomics Consortium and Buchmann Institute for Molecular Life Sciences, Institute for Pharmaceutical Chemistry, Johann Wolfgang Goethe-University, 60438 Frankfurt am Main, Germany

C. John Harris – CJH Consultants, Ford Cottage, Brockenhurst, Hants SO42 7UQ, U.K.

Brendan Leighton – The Research Network, Sandwich CT13 9NJ, U.K.

Steven P. Vickers – RenaSci Limited, Nottingham NG1 1GF, U.K.

Sharon C. Cheetham – RenaSci Limited, Nottingham NG1 1GF, U.K.

Colin Kenyon – DST/NRF Centre of Excellence for Biomedical Tuberculosis Research, SAMRC Centre for Molecular and Cellular Biology, Division of Molecular Biology and Human Genetics, Faculty of Medicine and Health Sciences, Stellenbosch University, Cape Town 8000, South Africa

Anna M. Grabowska – Ex Vivo Cancer Pharmacology Centre of Excellence, Cancer Biology, Division of Cancer and Stem Cells, School of Medicine, University of Nottingham, Nottingham NG7 2RD, U.K.

Michael Overduin – Department of Biochemistry, University of Alberta, Edmonton, Alberta T6G 2H7, Canada

Fedor Berdichevski – Institute of Cancer and Genomic Sciences, University of Birmingham, Birmingham B15 2TT, U.K.

Chris J. Weston – Centre for Liver Research, Institute of Immunology and Immunotherapy, University of Birmingham, Birmingham B15 2TT, U.K.; NIHR Birmingham Biomedical Research Centre, University Hospitals Birmingham NHS Foundation Trust and University of Birmingham, Birmingham B15 2TT, U.K.

Stefan Knapp – Structural Genomics Consortium and Buchmann Institute for Molecular Life Sciences, Institute for Pharmaceutical Chemistry, Johann Wolfgang Goethe-University, 60438 Frankfurt am Main, Germany; orcid.org/0000-0001-5995-6494

Peter M. Fischer – Centre for Biomolecular Sciences and School of Pharmacy, University of Nottingham, Nottingham NG7 2RD, U.K.; orcid.org/0000-0002-5866-9271

Complete contact information is available at:
<https://pubs.acs.org/10.1021/acs.jmedchem.9b01803>

Author Contributions

Compounds were designed and synthesized by C.F., A.A., D.K., L.H., G.G., A.C., H.V.N., D.H.J., M.G.S., A.V.R., B.S., G.P.I., C.J.H., P.M.F., and S.B. *In vitro* biology studies were designed and performed by M.L., S.R., C.B., J.K., P.G., V.N., J.M., A.C.R., A.K., C.K., M.O., S.K., and F.B. Crystal structure analysis was

performed by F.S. and A.K. *In vivo* DIO mice studies were designed by S.B., B.L., C.J.W., S.C.C., and S.P.V. The data obtained were interpreted by all authors. All authors have given approval to the final version of the manuscript.

Funding

This work was supported by the Wellcome Trust [103022 and 202708] and MRC [MC_PC_15032]. C.J.W. is funded by the NIHR Birmingham Biomedical Research Centre at the University Hospitals Birmingham, NHS Foundation Trust, and the University of Birmingham. This paper presents independent research supported by the NIHR Birmingham Biomedical Research Centre at the University Hospitals Birmingham NHS Foundation Trust and the University of Birmingham.

Notes

The views expressed are those of the author(s) and not necessarily those of the NHS, the NIHR, or the Department of Health and Social Care. *In vivo* studies were conducted in the UK in accordance with the Animal Ethical Review Group, University of Birmingham, and UK Home Office legislation, the Animal Scientific Procedures Act 1986, under Home Office project licenses 70/8420 (Saretius, PK studies) and 30/3208 (RenaSci, efficacy studies in DIO mice).

The authors declare no competing financial interest.

ACKNOWLEDGMENTS

KINOMEScan TREEspot images generated using TREEspot Software Tool and reprinted with permission from KINOMEScan, a division of DiscoverX Corporation, Copyright 2010 DISCOVERX CORPORATION. DIO mice studies were conducted by RenaSci (Nottingham, UK). Marvin, Calculator Plugins, and JChem Base were used for drawing, displaying, and characterizing chemical structures, structure searching, and chemical database access and management, ChemAxon (<http://www.chemaxon.com>).

ABBREVIATIONS

CaMK1, calmodulin-dependent kinase; GWAS, genome-wide association studies; FOXA1, hepatocyte nuclear factor 3- α ; siRNA, small interfering ribonucleic acid; CRTC2/TORC2, CREB regulated transcription coactivator 2; TNBC, triple-negative breast cancer; SYK, spleen tyrosine kinase; DIO, diet-induced obese; OGTT, oral glucose tolerance test

REFERENCES

- (1) Parkinson, H.; Kapushesky, M.; Shojatalab, M.; Abeygunawardena, N.; Coulson, R.; Farne, A.; Holloway, E.; Kolesnykov, N.; Lilja, P.; Lukk, M.; Mani, R.; Rayner, T.; Sharma, A.; William, E.; Sarkans, U.; Brazma, A. Array Express—a Public Database of Microarray Experiments and Gene Expression Profiles. *Nucleic Acids Res.* **2007**, *35* (Database), D747–750.
- (2) Wayman, G. A.; Lee, Y.-S.; Tokumitsu, H.; Silva, A.; Soderling, T. R. Calmodulin-Kinases: Modulators of Neuronal Development and Plasticity. *Neuron* **2008**, *59* (6), 914–931.
- (3) Zeggini, E.; Scott, L. J.; Saxena, R.; Voight, B. F.; Marchini, J. L.; Hu, T.; de Bakker, P. I.; Abecasis, G. R.; Almgren, P.; Andersen, G.; Ardlie, K.; Boström, K. B.; Bergman, R. N.; Bonnycastle, L. L.; Borch-Johnsen, K.; Burtt, N. P.; Chen, H.; Chines, P. S.; Daly, M. J.; Deodhar, P.; Ding, C. J.; Doney, A. S.; Duren, W. L.; Elliott, K. S.; Erdos, M. R.; Frayling, T. M.; Freathy, R. M.; Gianniny, L.; Grallert, H.; Grarup, N.; Groves, C. J.; Guiducci, C.; Hansen, T.; Herder, C.; Hitman, G. A.; Hughes, T. E.; Isomaa, B.; Jackson, A. U.; Jørgensen, T.; Kong, A.; Kubalanza, K.; Kuruvilla, F. G.; Kuusisto, J.; Langenberg, C.; Lango, H.; Lauritzen, T.; Li, Y.; Lindgren, C. M.; Lyssenko, V.; Maravelle, A. F.;

- Meisinger, C.; Midthjell, K.; Mohlke, K. L.; Morken, M. A.; Morris, A. D.; Narisu, N.; Nilsson, P.; Owen, K. R.; Palmer, C. N.; Payne, F.; Perry, J. R.; Pettersen, E.; Platou, C.; Prokopenko, I.; Qi, L.; Qin, L.; Rayner, N. W.; Rees, M.; Roix, J. J.; Sandbaek, A.; Shields, B.; Sjögren, M.; Steinhorsdottir, V.; Stringham, H. M.; Swift, A. J.; Thorleifsson, G.; Thorsteinsdottir, U.; Timpson, N. J.; Tuomi, T.; Tuomilehto, J.; Walker, M.; Watanabe, R. M.; Weedon, M. N.; Willer, C. J.; Illig, T.; Hveem, K.; Hu, F. B.; Laakso, M.; Stefansson, K.; Pedersen, O.; Wareham, N. J.; Barroso, I.; Hattersley, A. T.; Collins, F. S.; Groop, L.; McCarthy, M. I.; Boehnke, M.; Altshuler, D.; Wellcome Trust Case Control Consortium. Meta-Analysis of Genome-Wide Association Data and Large-Scale Replication Identifies Additional Susceptibility Loci for Type 2 Diabetes. *Nat. Genet.* **2008**, *40* (5), 638–645.
- (4) Shu, X. O.; Long, J.; Cai, Q.; Qi, L.; Xiang, Y.-B.; Cho, Y. S.; Tai, E. S.; Li, X.; Lin, X.; Chow, W.-H.; Go, M. J.; Seielstad, M.; Bao, W.; Li, H.; Cornelis, M. C.; Yu, K.; Wen, W.; Shi, J.; Han, B. G.; Sim, X. L.; Liu, L.; Qi, Q.; Kim, H. L.; Ng, D. P.; Lee, J. Y.; Kim, Y. J.; Li, C.; Gao, Y. T.; Zheng, W.; Hu, F. B. Identification of New Genetic Risk Variants for Type 2 Diabetes. *PLoS Genet.* **2010**, *6* (9), No. e1001127.
- (5) Kooner, J. S.; Saleheen, D.; Sim, X.; Sehmi, J.; Zhang, W.; Frossard, P.; Been, L. F.; Chia, K.-S.; Dimas, A. S.; Hassanali, N.; Jafar, T.; Jowett, J. B.; Li, X.; Radha, V.; Rees, S. D.; Takeuchi, F.; Young, R.; Aung, T.; Basit, A.; Chidambaram, M.; Das, D.; Grundberg, E.; Hedman, A. K.; Hydrie, Z. I.; Islam, M.; Khor, C. C.; Kowlessur, S.; Kristensen, M. M.; Liju, S.; Lim, W. Y.; Matthews, D. R.; Liu, J.; Morris, A. P.; Nica, A. C.; Pinidiyapathirage, J. M.; Prokopenko, I.; Rasheed, A.; Samuel, M.; Shah, N.; Shera, A. S.; Small, K. S.; Suo, C.; Wickremasinghe, A. R.; Wong, T. Y.; Yang, M.; Zhang, F.; Abecasis, G. R.; Barnett, A. H.; Caulfield, M.; Deloukas, P.; Frayling, T. M.; Froguel, P.; Kato, N.; Katulanda, P.; Kelly, M. A.; Liang, J.; Mohan, V.; Sanghera, D. K.; Scott, J.; Seielstad, M.; Zimmet, P. Z.; Elliott, P.; Teo, Y. Y.; McCarthy, M. I.; Danesh, J.; Tai, E. S.; Chambers, J. C.; Diabetes Genetics Replication And Meta-analysis (DIAGRAM) Consortium; MuTHER Consortium. Genome-Wide Association Study in Individuals of South Asian Ancestry Identifies Six New Type 2 Diabetes Susceptibility Loci. *Nat. Genet.* **2011**, *43* (10), 984–989.
- (6) Morris, A. P.; Voight, B. F.; Teslovich, T. M.; Ferreira, T.; Segre, A. V.; Steinthorsdottir, V.; Strawbridge, R. J.; Khan, H.; Grallert, H.; Mahajan, A.; Prokopenko, I.; Kang, H. M.; Dina, C.; Esko, T.; Fraser, R. M.; Kanoni, S.; Kumar, A.; Lagou, V.; Langenberg, C.; Luan, J.; Lindgren, C. M.; Müller-Nurasyid, M.; Pechlivanis, S.; Rayner, N. W.; Scott, L. J.; Wiltshire, S.; Yengo, L.; Kinnunen, L.; Rossin, E. J.; Raychaudhuri, S.; Johnson, A. D.; Dimas, A. S.; Loos, R. J.; Vedantam, S.; Chen, H.; Florez, J. C.; Fox, C.; Liu, C. T.; Rybin, D.; Couper, D. J.; Kao, W. H.; Li, M.; Cornelis, M. C.; Kraft, P.; Sun, Q.; van Dam, R. M.; Stringham, H. M.; Chines, P. S.; Fischer, K.; Fontanillas, P.; Holmen, O. L.; Hunt, S. E.; Jackson, A. U.; Kong, A.; Lawrence, R.; Meyer, J.; Perry, J. R.; Platou, C. G.; Potter, S.; Rehnberg, E.; Robertson, N.; Sivapalaratnam, S.; Stancáková, A.; Stirrups, K.; Thorleifsson, G.; Tikkanen, E.; Wood, A. R.; Almgren, P.; Atalay, M.; Benediktsson, R.; Bonnycastle, L. L.; Burt, N.; Carey, J.; Charpentier, G.; Crenshaw, A. T.; Doney, A. S.; Dorkhan, M.; Edkins, S.; Emilsson, V.; Eury, E.; Forsen, T.; Gertow, K.; Gigante, B.; Grant, G. B.; Groves, C. J.; Guiducci, C.; Herder, C.; Hreidarsson, A. B.; Hui, J.; James, A.; Jonsson, A.; Rathmann, W.; Klopp, N.; Kravic, J.; Krjutskov, K.; Langford, C.; Leander, K.; Lindholm, E.; Lobbens, S.; Männistö, S.; Mirza, G.; Mühleisen, T. W.; Musk, B.; Parkin, M.; Rallidis, L.; Saramies, J.; Sennblad, B.; Shah, S.; Sigurdsson, G.; Silveira, A.; Steinbach, G.; Thorand, B.; Trakalo, J.; Veglia, F.; Wennauer, R.; Winckler, W.; Zabaneh, D.; Campbell, H.; van Duijn, C.; Uitterlinden, A. G.; Hofman, A.; Sijbrands, E.; Abecasis, G. R.; Owen, K. R.; Zeggini, E.; Trip, M. D.; Forouhi, N. G.; Syvänen, A. C.; Eriksson, J. G.; Peltonen, L.; Nöthen, M. M.; Balkau, B.; Palmer, C. N.; Lyssenko, V.; Tuomi, T.; Isomaa, B.; Hunter, D. J.; Qi, L.; Shuldiner, A. R.; Roden, M.; Barroso, I.; Wilsgaard, T.; Beilby, J.; Hovingh, K.; Price, J. F.; Wilson, J. F.; Rauramaa, R.; Lakka, T. A.; Lind, L.; Dedoussis, G.; Njølstad, I.; Pedersen, N. L.; Khaw, K. T.; Wareham, N. J.; Keinanen-Kiukkaanniemi, S. M.; Saaristo, T. E.; Korpi-Hyövälti, E.; Saltevo, J.; Laakso, M.; Kuusisto, J.; Metspalu, A.; Collins, F. S.; Mohlke, K. L.; Bergman, R. N.; Tuomilehto, J.; Boehm, B. O.; Gieger, C.; Hveem, K.; Cauchi, S.; Froguel, P.; Baldassarre, D.; Tremoli, E.; Humphries, S. E.; Saleheen, D.; Danesh, J.; Ingelsson, E.; Ripatti, S.; Salomaa, V.; Erbel, R.; Jöckel, K. H.; Moebus, S.; Peters, A.; Illig, T.; de Faire, U.; Hamsten, A.; Morris, A. D.; Donnelly, P. J.; Frayling, T. M.; Hattersley, A. T.; Boerwinkle, E.; Melander, O.; Kathiresan, S.; Nilsson, P. M.; Deloukas, P.; Thorsteinsdottir, U.; Groop, L. C.; Stefansson, K.; Hu, F.; Pankow, J. S.; Dupuis, J.; Meigs, J. B.; Altshuler, D.; Boehnke, M.; McCarthy, M. I.; Diabetes Genetics Replication And Meta-analysis (DIAGRAM) Consortium; Wellcome Trust Case Control Consortium; Meta-Analysis of Glucose and Insulin-related traits Consortium (MAGIC) Investigators; Genetic, Investigation of ANthropometric, Traits (GIANT) Consortium; Asian Genetic Epidemiology Network—Type 2 Diabetes (AGEN-T2D) Consortium; South Asian Type 2 Diabetes (SAT2D) Consortium. Large-Scale Association Analysis Provides Insights into the Genetic Architecture and Pathophysiology of Type 2 Diabetes. *Nat. Genet.* **2012**, *44* (9), 981–990.
- (7) Fogarty, M. P.; Cannon, M. E.; Vadlamudi, S.; Gaulton, K. J.; Mohlke, K. L. Identification of a Regulatory Variant That Binds FOXA1 and FOXA2 at the CDC123/CAMK1D Type 2 Diabetes GWAS Locus. *PLoS Genet.* **2014**, *10* (9), No. e1004633.
- (8) Haney, S.; Zhao, J.; Tiwari, S.; Eng, K.; Guey, L. T.; Tien, E. RNAi Screening in Primary Human Hepatocytes of Genes Implicated in Genome-Wide Association Studies for Roles in Type 2 Diabetes Identifies Roles for CAMK1D and CDKAL1, among Others, in Hepatic Glucose Regulation. *PLoS One* **2013**, *8* (6), No. e64946.
- (9) Saberi, M.; Bjelica, D.; Schenk, S.; Imamura, T.; Bandyopadhyay, G.; Li, P.; Jadhav, V.; Vargeese, C.; Wang, W.; Bowman, K.; Zhang, Y.; Polisky, B.; Olefsky, J. M. Novel Liver-Specific TORC2 siRNA Corrects Hyperglycemia in Rodent Models of Type 2 Diabetes. *Am. J. Physiol. Metab.* **2009**, *297* (5), E1137–E1146.
- (10) Wang, Y.; Inoue, H.; Ravnskjaer, K.; Viste, K.; Miller, N.; Liu, Y.; Hedrick, S.; Vera, L.; Montminy, M. Targeted Disruption of the CREB Coactivator *Crtc2* Increases Insulin Sensitivity. *Proc. Natl. Acad. Sci. U. S. A.* **2010**, *107* (7), 3087–3092.
- (11) Erion, D. M.; Kotas, M. E.; McGlashan, J.; Yonemitsu, S.; Hsiao, J. J.; Nagai, Y.; Iwasaki, T.; Murray, S. F.; Bhanot, S.; Cline, G. W.; Samuel, V. T. CAMP-Responsive Element-Binding Protein (CREB)-Regulated Transcription Coactivator 2 (*CRTC2*) Promotes Glucagon Clearance and Hepatic Amino Acid Catabolism to Regulate Glucose Homeostasis. *J. Biol. Chem.* **2013**, *288* (22), 16167–16176.
- (12) Loo, L. W. M.; Wang, Y.; Flynn, E. M.; Lund, M. J.; Bowles, E. J. A.; Buist, D. S. M.; Liff, J. M.; Flagg, E. W.; Coates, R. J.; Eley, J. W.; Hsu, L.; Porter, P. L. Genome-Wide Copy Number Alterations in Subtypes of Invasive Breast Cancers in Young White and African American Women. *Breast Cancer Res. Treat.* **2011**, *127* (1), 297–308.
- (13) Shavers, V. L.; Harlan, L. C.; Stevens, J. L. Racial/Ethnic Variation in Clinical Presentation, Treatment, and Survival among Breast Cancer Patients under Age 35. *Cancer* **2003**, *97* (1), 134–147.
- (14) Bergamaschi, A.; Kim, Y. H.; Kwei, K. A.; La Choi, Y.; Bocanegra, M.; Langerød, A.; Han, W.; Noh, D.-Y.; Huntsman, D. G.; Jeffrey, S. S.; Borresen-Dale, A.-L.; Pollack, J. R. CAMK1D Amplification Implicated in Epithelial-Mesenchymal Transition in Basal-like Breast Cancer. *Mol. Oncol.* **2008**, *2* (4), 327–339.
- (15) Yamada, T.; Suzuki, M.; Satoh, H.; Kihara-Negishi, F.; Nakano, H.; Oikawa, T. Effects of PU.1-Induced Mouse Calcium-Calmodulin-Dependent Kinase I-like Kinase (CKL1K) on Apoptosis of Murine Erythroleukemia Cells. *Exp. Cell Res.* **2004**, *294* (1), 39–50.
- (16) Hisamichi, H.; Naito, R.; Toyoshima, A.; Kawano, N.; Ichikawa, A.; Orita, A.; Orita, M.; Hamada, N.; Takeuchi, M.; Ohta, M.; Tsukamoto, S.-i. Synthetic Studies on Novel Syk Inhibitors. Part 1: Synthesis and Structure–Activity Relationships of Pyrimidine-5-Carboxamide Derivatives. *Bioorg. Med. Chem.* **2005**, *13* (16), 4936–4951.
- (17) Liddle, J.; Atkinson, F. L.; Barker, M. D.; Carter, P. S.; Curtis, N. R.; Davis, R. P.; Douault, C.; Dickson, M. C.; Elwes, D.; Garton, N. S.; Gray, M.; Hayhow, T. G.; Hobbs, C. I.; Jones, E.; Leach, S.; Leavens, K.; Lewis, H. D.; McCleary, S.; Neu, M.; Patel, V. K.; Preston, A. G.; Ramirez-Molina, C.; Shipley, T. J.; Skone, P. A.; Smithers, N.; Somers,

D. O.; Walker, A. L.; Watson, R. J.; Weingarten, G. G. Discovery of GSK143, a Highly Potent, Selective and Orally Efficacious Spleen Tyrosine Kinase Inhibitor. *Bioorg. Med. Chem. Lett.* **2011**, *21* (20), 6188–6194.

(18) Thoma, G.; Smith, A. B.; van Eis, M. J.; Vangrevelinghe, E.; Blanz, J.; Aichholz, R.; Littlewood-Evans, A.; Lee, C. C.; Liu, H.; Zerwes, H.-G. Discovery and Profiling of a Selective and Efficacious Syk Inhibitor. *J. Med. Chem.* **2015**, *58* (4), 1950–1963.

(19) Ellis, J. M.; Altman, M. D.; Bass, A.; Butcher, J. W.; Byford, A. J.; Donofrio, A.; Galloway, S.; Haidle, A. M.; Jewell, J.; Kelly, N.; Leccese, E. K.; Lee, S.; Maddess, M.; Miller, J. R.; Moy, L. Y.; Osimboni, E.; Otte, R. D.; Reddy, M. V.; Spencer, K.; Sun, B.; Vincent, S. H.; Ward, G. J.; Woo, G. H.; Yang, C.; Houshyar, H.; Northrup, A. B. Overcoming Mutagenicity and Ion Channel Activity: Optimization of Selective Spleen Tyrosine Kinase Inhibitors. *J. Med. Chem.* **2015**, *58* (4), 1929–1939.

(20) Gao, Y.; Davies, S. P.; Augustin, M.; Woodward, A.; Patel, U. A.; Kovelman, R.; Harvey, K. J. A Broad Activity Screen in Support of a Chemogenomic Map for Kinase Signalling Research and Drug Discovery. *Biochem. J.* **2013**, *451* (2), 313–328.

(21) Shang, R.; Ji, D.-S.; Chu, L.; Fu, Y.; Liu, L. Synthesis of α -Aryl Nitriles through Palladium-Catalyzed Decarboxylative Coupling of Cyanoacetate Salts with Aryl Halides and Triflates. *Angew. Chem., Int. Ed.* **2011**, *50* (19), 4470–4474.